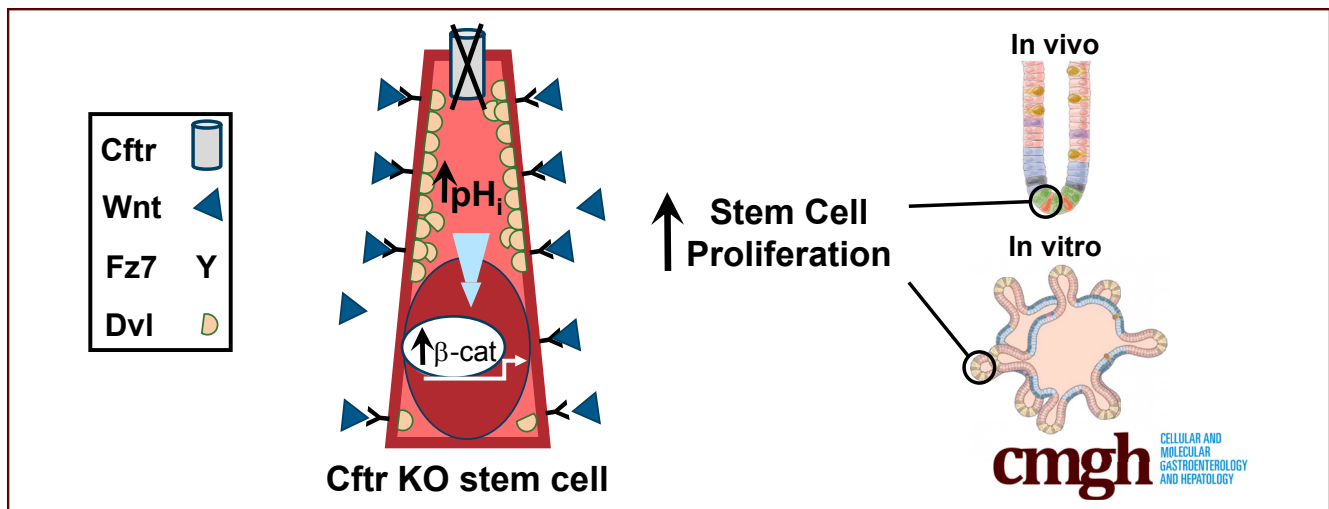


## ORIGINAL RESEARCH

Cftr Modulates Wnt/ $\beta$ -Catenin Signaling and Stem Cell Proliferation in Murine Intestine

Ashlee M. Strubberg,<sup>1</sup> Jinghua Liu,<sup>2</sup> Nancy M. Walker,<sup>2</sup> Casey D. Stefanski,<sup>1</sup> R. John MacLeod,<sup>3</sup> Scott T. Magness,<sup>4</sup> and Lane L. Clarke<sup>1,2</sup>

<sup>1</sup>Department of Biomedical Sciences, <sup>2</sup>Dalton Cardiovascular Research Center, University of Missouri, Columbia, Missouri; <sup>3</sup>Department of Biomedical and Molecular Sciences, Queen's University, Kingston, Ontario, Canada; <sup>4</sup>Department of Medicine, Department of Cell and Molecular Physiology, University of North Carolina at Chapel Hill, Chapel Hill, North Carolina



## SUMMARY

This study documents the functional activity of cystic fibrosis transmembrane conductance regulator (Cftr) in the active intestinal stem cell population of murine intestine. In the absence of Cftr, the intracellular pH, inner membrane localization of the Wnt-transducer Dishevelled, Wnt/ $\beta$ -catenin signaling, and stem cell proliferation are all increased, which may contribute to increased gastrointestinal cancer risk in cystic fibrosis.

**BACKGROUND & AIMS:** Cystic fibrosis (CF) patients and CF mouse models have increased risk for gastrointestinal tumors. CF mice show augmented intestinal proliferation of unknown etiology and an altered intestinal environment. We examined the role of the cystic fibrosis transmembrane conductance regulator (Cftr) in Wnt/ $\beta$ -catenin signaling, stem cell proliferation, and its functional expression in the active intestinal stem cell (ISC) population. Dysregulation of intracellular pH (pH<sub>i</sub>) in CF ISCs was investigated for facilitation of Wnt/ $\beta$ -catenin signaling.

**METHODS:** Crypt epithelia from wild-type (WT) and CF mice were compared ex vivo and in intestinal organoids (enteroids) for proliferation and Wnt/ $\beta$ -catenin signaling by standard assays. Cftr in ISCs was assessed by immunoblot of sorted Sox9<sup>enhanced green fluorescent protein(EGFP)</sup> intestinal epithelia and

pH<sub>i</sub> regulation by confocal microfluorimetry of leucine-rich G-protein-coupled receptor 5 ISCs. Plasma membrane association of the Wnt transducer Dishevelled 2 (Dvl2) was assessed by fluorescence imaging of live enteroids from WT and CF mice crossed with Dvl2-EGFP/ACTB-tdTomato,EGFP)Luo/J (Rosa<sup>mT/mG</sup>) mice.

**RESULTS:** Relative to WT, CF intestinal crypts showed an ~30% increase in epithelial and Lgr5+ ISC proliferation and increased Wnt/ $\beta$ -catenin signaling. Cftr was expressed in Sox9<sup>EGFP</sup> ISCs and loss of Cftr induced an alkaline pH<sub>i</sub> in ISCs. CF crypt-base columnar cells showed a generalized increase in plasma membrane Dvl2-EGFP association as compared with WT. Dvl2-EGFP membrane association was charge- and pH-dependent and increased in WT crypt-base columnar cells by Cftr inhibition.

**CONCLUSIONS:** CF intestine shows increased ISC proliferation and Wnt/ $\beta$ -catenin signaling. Loss of Cftr increases pH<sub>i</sub> in ISCs, which stabilizes the plasma membrane association of the Wnt transducer Dvl, likely facilitating Wnt/ $\beta$ -catenin signaling. Absence of Cftr-dependent suppression of ISC proliferation in the CF intestine may contribute to increased risk for intestinal tumors. (*Cell Mol Gastroenterol Hepatol* 2018;5:253-271; <https://doi.org/10.1016/j.jcmgh.2017.11.013>)

**Keywords:** Cystic Fibrosis; Dishevelled; Organoids; Intracellular pH; Neoplasia.

See editorial on page 418.

Cystic fibrosis (CF) is a heritable genetic disease caused by mutations in the cystic fibrosis transmembrane conductance regulator (CFTR) gene. The gene product (CFTR) is a major anion channel of fluid transporting epithelia where it functions in transepithelial  $\text{Cl}^-$  and  $\text{HCO}_3^-$  secretion.<sup>1,2</sup> CF affects multiple organs, in particular the airway epithelia where failure of mucociliary clearance results in bacterial colonization of the lung. However, intestinal disease is one of the earliest manifestations of CF and presents with life-long conditions, including small intestinal bacterial overgrowth,<sup>3</sup> low-grade small-bowel inflammation,<sup>4,5</sup> obstructive bowel disease,<sup>6,7</sup> and an increased incidence of gastrointestinal (GI) cancer.<sup>8,9</sup> Cftr knockout (KO) mice recapitulate CF intestinal disease without significant manifestations of pancreatic, liver, or lung disease. The disease phenotype includes a high incidence of bowel obstruction,<sup>10</sup> low-grade bowel inflammation,<sup>11</sup> small intestinal bacterial overgrowth,<sup>3</sup> dysbiosis,<sup>12</sup> and the spontaneous development of intestinal tumors with age.<sup>13</sup>

Previous *in vivo* studies have shown that Cftr KO mice show increased intestinal epithelial proliferation without a corresponding increase in apoptosis,<sup>14</sup> a condition that may predispose to intestinal neoplasia.<sup>15</sup> Recent epidemiologic studies have shown strong correlations between the rate of stem cell division and the incidence of cancer.<sup>16</sup> Because the intestine has one of the highest rates of epithelial turnover in the body, pathologic manifestations of CF that enhance the rate of epithelial turnover and contribute to intestinal inflammation are predicted to increase the risk of GI cancer. However, a mechanistic understanding linking the absence of Cftr with enhanced proliferation of the intestinal epithelium, particularly the stem cell population, has not been advanced.

Cftr is highly expressed in intestinal crypts,<sup>17,18</sup> the proliferative compartment of the intestine, and by providing apical membrane  $\text{Cl}^-$  and  $\text{HCO}_3^-$  ion permeability has an impact on the regulation of epithelial intracellular pH ( $\text{pH}_i$ ). Loss of Cftr function by acute channel blockade or in Cftr KO enteroids results in an incompletely compensated alkaline  $\text{pH}_i$  in the crypt epithelium.<sup>19</sup> Compensation of the alkaline  $\text{pH}_i$  is impaired by a corresponding increase in intracellular  $\text{Cl}^-$  concentration, which reduces cellular anion exchange activity.<sup>20</sup> Several aspects of cell proliferation are known to be facilitated by an alkaline  $\text{pH}_i$ , including cell-cycle phase progression at G2/M,<sup>21</sup> optimization of DNA replication,<sup>22</sup> cytoskeleton remodeling and cell migration,<sup>23,24</sup> and membrane biogenesis.<sup>25</sup> Cell alkalinity also has been shown to facilitate Wnt signaling,<sup>26,27</sup> which may directly affect stem cell proliferation.

Wnt/ $\beta$ -catenin signaling is essential for homeostasis and proliferation of intestinal stem cells<sup>28</sup> and often aberrantly is activated in intestinal cancer. In *Drosophila* species,  $\text{pH}_i$  changes can alter Wnt signaling by modulating the interaction of the initial signal mediator Dishevelled (Dsh) with the Wnt receptor Frizzled (Fz) at the plasma membrane.<sup>26</sup> The critical binding of Dvl's post synaptic density protein, *Drosophila* disc large tumor suppressor and Zonula

occludens-1 protein (PDZ) domain with the PDZ binding domain of Fz is facilitated by a stable interaction of Dvl's polybasic Dishevelled, Egl-10, and Pleckstrin (DEP) domain to negatively charged phospholipids (phosphatidic acid, phosphatidylglycerol) at the inner leaflet of the plasma membrane. Phospholipid interaction is  $\text{pH}_i$ - and charge-dependent such that proton electrostatic interference at an acidic  $\text{pH}_i$  reduces DEP domain membrane binding and subsequent Wnt signaling.<sup>26</sup> We hypothesized that an alkaline  $\text{pH}_i$  in Cftr KO intestinal stem cells stabilizes Dvl interaction at the plasma membrane, thereby facilitating Wnt/ $\beta$ -catenin signaling.

The present study investigated augmented proliferation of the intestinal epithelium in a Cftr KO mouse model. Studies examined whether hyperproliferation persists in Cftr KO enteroid culture, which isolates the epithelium from the immediate consequences of an abnormal Cftr KO intestinal environment (inflammation, dysbiosis) and provides the technological advantage of live crypt cell imaging.<sup>3,11,29</sup> Second, studies evaluated the activation status of Wnt/ $\beta$ -catenin signaling in the Cftr KO intestine and the functional activity of Cftr in ISCs, specifically, leucine-rich G-protein-coupled receptor 5 (Lgr5) stem cells.<sup>30</sup> Third, live cell imaging was used to examine the hypothesis that alkalinity of Cftr KO intestinal crypt base columnar stem cells was conducive to increased interaction of Dvl (ie, the major isoform Dvl2<sup>31</sup>) with the plasma membrane for Wnt signaling.

## Materials and Methods

### Mice

Mice with gene targeted disruptions of the murine homolog of Cftr (*abcc7*, Cftr KO) and sex-matched wild-type (WT, +/+ or +/-) littermates were used.<sup>10</sup> Mice were outbred to Black Swiss (Charles River, Wilmington, MA) mice at generational intervals and resultant F1 heterozygotes were crossed to generate F2 offspring for experimentation. The Cftr KO mouse line was crossed with Lgr5-enhanced green fluorescent protein (EGFP)-IRES-creERT2 (Lgr5-EGFP; Jackson Laboratories, Bar Harbor, ME) mice to generate WT/Lgr5-EGFP and Cftr KO/Lgr5-EGFP mice. The Cftr KO mouse line also was crossed with both Dvl2 KO/Dvl2-EGFP BAC transgenic<sup>32</sup> and Gt(ROSA)<sup>26Sortm4(ACTB-tdTomato,-EGFP)<sup>Luo</sup>/J</sup> (*Rosa*<sup>mT/mG</sup>; Jackson Laboratories) mouse lines to generate WT and Cftr KO/

**Abbreviations used in this paper:** CBC, crypt-base columnar cell; CCH, carbachol; CF, cystic fibrosis; Cftr, cystic fibrosis transmembrane conductance regulator; DEP, Dishevelled, Egl-10, and Pleckstrin; Dvl, Dishevelled; EdU, 5-ethynyl-2'-deoxyuridine; EGFP, enhanced green fluorescent protein; Fz, Frizzled; GI, gastrointestinal; ISC, intestinal stem cell; KO, knockout; Lgr5, leucine-rich G-protein-coupled receptor 5; PBS, phosphate-buffered saline; PDZ, Post synaptic density protein, *Drosophila* disc large tumor suppressor, and Zonula occludens-1 protein;  $\text{pH}_i$ , intracellular pH; PH3, phospho-histone H3; ROI, region of interest; WT, wild type.

 Most current article

© 2018 The Authors. Published by Elsevier Inc. on behalf of the AGA Institute. This is an open access article under the CC BY-NC-ND license (<http://creativecommons.org/licenses/by-nc-nd/4.0/>).

2352-345X

<https://doi.org/10.1016/j.jcmgh.2017.11.013>

Dvl2 KO/Dvl2-EGFP/Rosa<sup>mT/mG</sup> mice. Genotypes were identified by polymerase chain reaction analysis of tail-snip DNA as previously described for mutant Cftr,<sup>33</sup> Dvl2 KO and Dvl2-EGFP expression,<sup>34</sup> and Rosa<sup>mT/mG</sup> (Jackson Laboratories). Copy number for the Dvl2-EGFP transgene was verified by TaqMan GFP copy number assay (ThermoFisher Scientific, Waltham, MA). Only mice expressing 2 copies of the Dvl2-EGFP transgene were used for experimental analysis. All mice were maintained ad libitum on standard laboratory chow (Formulab 5008, Rodent Chow; Nestle Purina, St. Louis, MO) and distilled water containing Colyte (Schwartz Pharma, Mequon, WI) laxative to prevent intestinal obstruction in the Cftr KO mice. Mice were housed individually in a temperature- and light-controlled room (22°C–26°C; 12-hour light:12-hour dark cycle) in the Association for Assessment and Accreditation of Laboratory Animal Care-accredited animal facility at the Dalton Cardiovascular Research Center at the University of Missouri. Mouse experiments were performed in accordance with guidelines outlined in the Guide for the Care and Use of Laboratory Animals prepared by the National Academy of Sciences and published by the National Institutes of Health and with approval from the University of Missouri Institutional Animal Care and Use Committee.

### Enteroid Culture

The enteroid culture of isolated crypt epithelium from the proximal jejunum has been described previously in detail.<sup>19</sup> Cultures were overlaid with growth medium containing Ham's F-12 medium with 5% fetal bovine serum, 50 µg/mL gentamicin, 125 ng/mL R-spondin1, 25 ng/mL noggin, and 12.5 ng/mL epidermal growth factor. Growth medium was changed every 3–4 days and enteroids were passaged every 7–10 days using Cell Recovery Solution (BD Sciences, San Jose, CA). Except where otherwise indicated, passages 1–2 were used for experimentation.

### Lgr5-EGFP Cell Counts

Crypts were isolated from WT/Lgr5-EGFP or Cftr KO/Lgr5-EGFP mice and fixed immediately in 10% buffered formalin (Sigma-Aldrich, St. Louis, MO), or cultured as enteroids in growth medium before fixation. Z-stack images were acquired using either a TCS SP5 confocal-multiphoton microscope built on a DMI6000 inverted platform (Leica, Wetzlar, Germany) or an Olympus (Waltham, MA) Fluoview confocal microscope (FV1000). Images were reconstructed 3-dimensionally using Imaris Software (version 7.7.1; Bitplane, Concord, MA), and the number of Lgr5-EGFP-positive stem cells identified in 3 dimensions was counted for each crypt.

### Immunofluorescence

Freshly isolated crypts or enteroids from the proximal jejunum were fixed in 10% buffered formalin (Sigma-Aldrich) or 4% paraformaldehyde and stored at 4°C until processing. Fixed enteroids and Matrigel (Corning, Corning, NY) were scraped from the culture dishes, transferred to 1.5-mL tubes, centrifuged at 200g (1 min), and washed 3 times with 1× phosphate-buffered saline (PBS) to remove Matrigel and fixative. Samples were permeabilized for 60 minutes using

0.5% Triton X-100 (Sigma-Aldrich) in PBS and blocked for 30 minutes with gentle shaking in fish skin gelatin buffer (10 mmol/L Tris, 5 mmol/L EDTA, 0.15 mol/L NaCl, 0.25% fish skin gelatin [Sigma-Aldrich], and 0.05% Tween20). Samples were incubated overnight at 4°C with primary antibody diluted in fish skin gelatin buffer, washed 3 times in fish skin gelatin buffer, and incubated with secondary antibody for 4–5 hours with gentle shaking at 4°C. After removal of the secondary antibody, samples were washed 3 times for 10 minutes in fish skin gelatin buffer. Samples then were resuspended in SlowFade gold antifade mounting medium (ThermoFisher Scientific) and sealed under glass coverslips on microscope slides (ThermoFisher Scientific). Fresh crypts and enteroids were imaged using an Olympus Fluoview confocal microscope. Z-stacks were imaged to determine crypt cross-sections after acquisition using Imaris Software. Anti-Frizzled 7 (10 µg/mL, AF198; R&D Systems, Minneapolis, MN) was used as primary antibody and secondary antibody was anti-goat IgG Alexa Fluor 405 (ab175665; Abcam, Cambridge, MA) used at a 1:500 dilution in fish skin gelatin buffer.

### Proliferation Assays

Proliferation of WT and Cftr KO freshly isolated crypts was measured by immunofluorescence for mitotic cells using anti-phospho-histone H3 (PH3) primary antibody (1:100 dilution, 06-570; Millipore) in fish skin gelatin buffer (see Immunofluorescence). Nuclei were labeled with TO-PRO 3 (ThermoFisher Scientific) nuclear stain (1:2000 dilution) in fish skin gelatin buffer. Proliferation of enteroid crypts (passage 1 or passage 2, 5–7 days) maintained in growth medium was measured using 5-ethynyl-2'-deoxyuridine (EdU) to label cells in the S phase of the cell cycle. Enteroids were exposed in situ to EdU for 15 minutes, fixed in 4% paraformaldehyde, and stored at 4°C. Fixed enteroids and Matrigel were scraped from the culture dishes, transferred into 1.5-mL tubes, and centrifuged at 200g for 1 minute. The supernatant containing Matrigel was aspirated and the fixed enteroids were washed twice with 1× PBS. The Click-iT EdU assay was performed according to the manufacturer's protocol (ThermoFisher Scientific) and as previously described.<sup>35</sup> Nuclei were labeled with Hoechst 33342 diluted 1:2000 for 1 hour. Labeled enteroids were concentrated by brief centrifugation (200g, 1 min), resuspended in SlowFade gold antifade mounting medium (ThermoFisher Scientific), and sealed under a glass coverslip on microscope slides. Crypts were imaged on an Olympus Fluoview confocal microscope (FV1000). Post-acquisition 3D reconstructed Z-stacks (Imaris Software) were used to determine crypt cross-sections for counting PH3-positive (PH3+), EdU-positive (EdU+), and total nuclei. Acquired images were coded and nuclei counting was performed by an observer blinded to genotype.

### Immunoblot Analysis

Freshly isolated crypts, enteroids, or sorted intestinal epithelial cells were suspended in ice-cold, radio-immunoprecipitation assay buffer (Cell Signaling, Danvers, MA) containing Halt Protease inhibitor (ThermoFisher Scientific) and lysed at 4°C by sonication. Total lysate protein

was loaded on 10% sodium dodecyl sulfate–polyacrylamide gels for electrophoresis, membrane transfer, and immunoblotting. Anti-active  $\beta$ -catenin (1:2000 dilution, 05-665; Millipore), anti-Lef1 (1:500 dilution, sc-28687; Santa Cruz, Dallas, TX), and anti-Cftr 3G11 (1:2000 dilution, provided by CFTR Folding Consortium, Cystic Fibrosis Foundation Therapeutics) were used as primary antibodies. Anti- $\beta$ -actin (1:2000 dilution, sc-130656; Santa Cruz) or anti-glyceraldehyde-3-phosphate dehydrogenase (1:2000 dilution, sc-25778; Santa Cruz) were used as loading controls. Densitometry was performed using Image Lab Software (version 5.2.1; BioRad).

### Fluorescence-Activated Cell Sorter

Isolated small intestinal crypt cells from Sox9<sup>EGFP</sup> mice were dissociated for fluorescence-activated cell sorting, as previously described.<sup>36</sup> Sox9<sup>EGFP<sup>Negative</sup></sup>, Sox9<sup>EGFP<sup>Sublo</sup></sup>, Sox9<sup>EGFP<sup>Lo</sup></sup>, and Sox9<sup>EGFP<sup>High</sup></sup> cells were isolated using a MoFlo fluorescence-activated cell sorter machine (Dako/Cytomation, Glostrup, Denmark). Cells were collected in radioimmunoprecipitation assay buffer and frozen at -20°C for protein immunoblotting.

### Confocal Microfluorimetry of Intracellular pH

WT, Cftr KO, WT/Lgr5-EGFP, and Cftr KO/Lgr5-EGFP enteroids were cultured in growth medium for 5–7 days on glass-bottomed Fluorodishes (World Precision Instruments, Sarasota, FL). Enteroids were loaded with the ratiometric pH-sensitive dye SNARF-5F (ThermoFisher Scientific) at 40  $\mu$ mol/L for 30 minutes at 37°C as previously described.<sup>19</sup> For basal conditions, cultures were superfused continuously with Krebs's bicarbonate Ringer + 5 mmol/L N-tris(hydroxymethyl)-methyl-2-aminoethanesulfonic acid buffer and gassed with 95% O<sub>2</sub>:5% CO<sub>2</sub> (pH 7.4, 37°C). For Cftr KO enteroids grown in pH 7.1 or 6.6 medium, enteroids were imaged in static culture medium (pH 7.1 or 6.6) with an overlying 95% air:5% CO<sub>2</sub> atmosphere maintained at 37°C using a culture dish incubator (DH-35iL, 64-0349; Warner Instruments, Hamden, CT). All images were acquired with a TCS SP5 Leica confocal microscope in a temperature-controlled incubator. The excitation source for SNARF-5F was a 514-nm argon laser and images were collected at dual-emission wavelengths (580  $\pm$  30 and 640  $\pm$  30 nm). Z-stacks of individual crypts were imaged and regions of interest (ROIs) were placed after acquisition using Imaris Software. For intracellular regional pH<sub>i</sub> studies, ROIs were placed on cross-sectional slices at the apical aspect of crypt-base columnar cells (CBCs) near the +4 position (to avoid Paneth cell granule fluorescence) using SlideBook 5.0 (Intelligent Imaging Innovations, Denver, CO). The 580- to 640-nm ratio was converted to pH<sub>i</sub> using a standard curve generated by the K<sup>+</sup>/nigericin technique in unlabeled and Lgr5-EGFP-positive cells.<sup>37</sup>

### Live Imaging of Enteroids for Dvl2-EGFP Membrane Association

Passaged enteroids were plated in Matrigel onto Fluorodishes and cultured for 5–7 days before imaging. Unless indicated otherwise, enteroids were gassed with

95% air:5% CO<sub>2</sub> and maintained at 37°C using the culture incubator DH-35iL during all acquisitions. Z-stacks were acquired using an Olympus Fluoview 1000 confocal microscope. Postacquisition 3D reconstructed Z-stacks (Imaris Software) were used to determine crypt cross-sections for Dvl2-EGFP proximity to the plasma membrane of CBCs in live enteroid crypts. CBCs were selected based on the following: (1) location at cell positions 1–3; (2) lack of granulation as defined by the absence of a granule theca outlined by Rosa<sup>MT/mG</sup> label (prominent in Paneth or goblet cells) and lack of granules by light images; (3) a contiguous and well-defined Rosa<sup>MT/mG</sup>-labeled plasma membrane; and (4) not overtly undergoing cell division as indicated by a nuclear position apical to the basal membrane and membrane accumulation at the apical pole of the cell. Using ImageJ software (version 1.49; Bethesda, MD), preliminary studies indicated that Dvl2-EGFP intensity measurements taken at CBC plasma membrane adjacent to the nucleus were confounded technically (owing to minimal cytoplasm and curvature of the nucleus) and conceptually (apposition of nuclear and plasma membranes). Therefore, measurement of the juxtamembrane Dvl2-EGFP intensity was confined to the lateral membranes in the supranuclear portion of CBCs (ie, apical to the nucleus). Acquired images were coded and measurement of juxtamembrane Dvl2-EGFP was performed by an observer blinded to genotype. To quantitate membrane proximity of Dvl2-EGFP at the supranuclear lateral plasma membranes of CBC, the Rosa<sup>MT/mG</sup>-labeled lateral plasma membranes were outlined as a ROI on the red (mTomato) channel images of cell cross-sections using ImageJ software. The ROI was copied to the green (EGFP) channel image of the CBC for measurement of Dvl2-EGFP intensity within a 2-pixel distance (1.15  $\mu$ m) interior to the supranuclear lateral plasma membrane, and avoiding the apical (brush border) membrane. The average Dvl2-EGFP intensity of pixels also was acquired for the entire supranuclear region of each CBC. This measurement was used to normalize differences in EGFP intensity between CBCs by calculating the ratio of average juxtamembrane EGFP intensity divided by average EGFP intensity of all pixels in the supranuclear region of the CBC. Average EGFP intensity of pixels in the supranuclear region were not significantly different between WT and Cftr KO CBCs (average intensity: WT = 59.5  $\pm$  8.8, and Cftr KO = 88.5  $\pm$  15.9, not significant, n = 6–7, respectively). Because measurements of juxtamembrane apposition of Dvl2-EGFP were performed on 2D confocal slices of CBCs, EGFP intensity at the lateral membrane oriented lateral (lateral-Lateral) and medial (medial-Lateral) to the central axis of the crypt were also individually collected.

### Charge- and pH<sub>i</sub>-Dependence of Dvl2-EGFP Association With the Plasma Membrane in Cftr KO Enteroids

Cftr KO enteroids were treated with either sphingosine (Avanti Polar Lipids, Alabaster, AL), low bicarbonate medium, bumetanide plus carbachol (CCH; Sigma), or Cftr<sub>inh</sub>-172 (Sigma) plus GlyH-101 (Millipore) to alter Dvl2-EGFP

localization at the plasma membrane. For experiments using sphingosine to neutralize negative charges at the inner leaflet of the plasma membrane, Cftr KO enteroids were treated with sphingosine in growth medium for 1 hour before imaging (95% ethanol:5% water used as vehicle, 1:2000 final dilution). For experiments lowering  $pH_i$ , Cftr KO enteroids were cultured for 3 days in standard medium and then 2 days in either low bicarbonate medium (3.6 mmol/L bicarbonate, 7 mmol/L sodium N-tris[hydroxymethyl]-methyl-2-aminoethanesulfonic acid, 6.8 mmol/L mannitol, pH 6.6), or maintained in standard medium (14 mmol/L bicarbonate, pH 7.1). For experiments to acutely reduce intracellular  $Cl^-$  and  $pH_i$ , Cftr KO enteroids were sequentially treated with bumetanide (50  $\mu$ mol/L, Sigma; dissolved in dimethyl sulfoxide, DMSO) and CCH (100  $\mu$ mol/L), as previously described.<sup>20</sup> Briefly, Cftr KO enteroids were treated with bumetanide for 15 minutes to block  $Cl^-$  uptake by the basolateral sodium-potassium-two chloride cotransporter 1 (NKCC1) followed by co-treatment with CCH for 15 minutes to activate  $Cl^-$  efflux via  $Ca^{2+}$ -activated  $Cl^-$  channels, eg, anoctamin 1 (Ano1). The treatment lowers intracellular  $Cl^-$  concentration sufficiently to facilitate activity of the basolateral anion exchanger 2. In experiments to acutely block Cftr to increase  $pH_i$ , WT enteroids were treated for 1 hour with a combination of 10  $\mu$ mol/L Cftr<sub>inh</sub>-172 and 20  $\mu$ mol/L GlyH101 dissolved in dimethyl sulfoxide to evaluate changes in Dvl2-EGFP association with the plasma membrane. Measurements of Dvl2-EGFP intensity were performed by an observer blinded to treatment and genotype.

### Materials

EGF, noggin, and Wnt3a were obtained from R&D Systems. Recombinant Rspodin1 was isolated as described previously.<sup>38</sup>

### Statistics

Cumulative data are reported as the means  $\pm$  SE. Intracellular pH data are the average of individual Lgr5-EGFP or crypt-base columnar cells in crypts from WT or Cftr KO enteroids. For juxtamembrane Dvl2-EGFP measurement, individual mouse averages are shown for EGFP intensity, which are derived from the average of 1–3 crypt-base columnar cells/crypt from 2–4 crypts of both passage 1 and 2 enteroids. Significant differences between female and male mice were not found for measurements of  $pH_i$  in Lgr5-EGFP/crypt-base columnar cells or baseline membrane localization of Dvl2-EGFP, so these data were combined in the averages. Data between 2 groups were compared using a 2-tailed Student *t* test or, if not normally distributed with equal variances, by the Mann–Whitney rank sum test. A probability value of  $P < .05$  was considered statistically significant.

## Results

### Increased Intestinal Proliferation in Cftr KO Crypts Is Recapitulated in Early Passage Enteroids

Previous *in vivo* studies of the Cftr KO mouse intestine showed a 34% increase in epithelial proliferation measured

by proliferating cell nuclear antigen labeling without a change in apoptosis as compared with WT intestine.<sup>14</sup> To assess intestinal hyperproliferation in our Cftr KO mice *in vivo*, mitotic cells identified as PH3+ were enumerated by confocal microscopy using freshly isolated crypts from the proximal small intestine of Cftr KO and WT matched mice (Figure 1A). Cftr KO crypts had a 52% increase in the number of PH3+ cells per crypt optical cross-section. Mitotic figures were found in both crypt base ( $< +4$  cell position) and the transit-amplifying zone ( $> +4$  position) of each genotype, indicating enhanced proliferation in the ISC and progenitor cell populations. Crypt-base columnar cells represent the active ISC population and express the ISC marker Lgr5<sup>39</sup>; therefore, Cftr KO heterozygous mice were cross-bred with Lgr5-EGFP-ires-CreERT2 (Lgr5-EGFP) mice to compare the average number of Lgr5+ stem cells per crypt between genotypes.<sup>30</sup> By using freshly isolated crypts from WT/Lgr5-EGFP and Cftr KO/Lgr5-EGFP-matched mice, the number of Lgr5-EGFP-labeled cells was enumerated for each crypt containing at least 1 Lgr5-EGFP+ cell (Lgr5-EGFP expression is mosaic). As shown in Figure 1B, the average number of Lgr5-EGFP+ cells per crypt was significantly greater in the Cftr KO/Lgr5-EGFP intestine as compared with WT/Lgr5-EGFP intestine (30.4% increase in mean Lgr5-EGFP+/crypt).

Murine enteroids are well-differentiated, primary cultures of the small intestinal epithelium that can undergo multiple passages.<sup>30</sup> WT enteroid crypts express functional Cftr activity and have proliferation rates that recapitulate *in vivo* rates when grown as detailed in the Methods section<sup>19</sup> (ie, 25% growth factor concentration relative to the method of Sato et al<sup>30</sup>). Enteroids from WT and Cftr KO mice enable imaging of live cellular processes in real time. Furthermore, enteroids avoid the immediate consequences of the abnormal CF intestinal environment,<sup>3,10–12</sup> which includes inflammatory mediators and reparative processes that alter Wnt/ $\beta$ -catenin signaling and ISC proliferation.<sup>40,41</sup>

By using passage 1 and 2 cultures, WT and Cftr KO enteroids were exposed to EdU to enumerate cells in the S phase. As shown in Figure 1C, EdU incorporation showed a 37% increase in proliferation of Cftr KO enteroid crypts compared with WT, as assessed by increases in the total number of EdU+ cells and the percentage of EdU+ cells per crypt cross-section in the Cftr KO enteroid crypts. To estimate ISC proliferation, the number of Lgr5-EGFP+ cells in crypts containing at least 1 Lgr5-EGFP+ cell were enumerated in passage 1 enteroids from WT/Lgr5-EGFP and Cftr KO/Lgr5-EGFP-matched mice. As shown in Figure 1D, Lgr5-EGFP+ cells/crypt were significantly greater in the Cftr KO/Lgr5-EGFP as compared with WT/Lgr5-EGFP enteroids (44% increase in mean Lgr5-EGFP+/crypt).

We next asked whether later passages (ie, passage 4) of Cftr KO enteroids would maintain high rates of proliferation, thereby suggestive of an epithelial-autonomous effect of Cftr ablation. At passage 4, WT and Cftr KO enteroids showed similar proliferation rates as measured by EdU labeling. However, the change largely was owing to increased proliferation in the WT enteroid crypts, which changed from

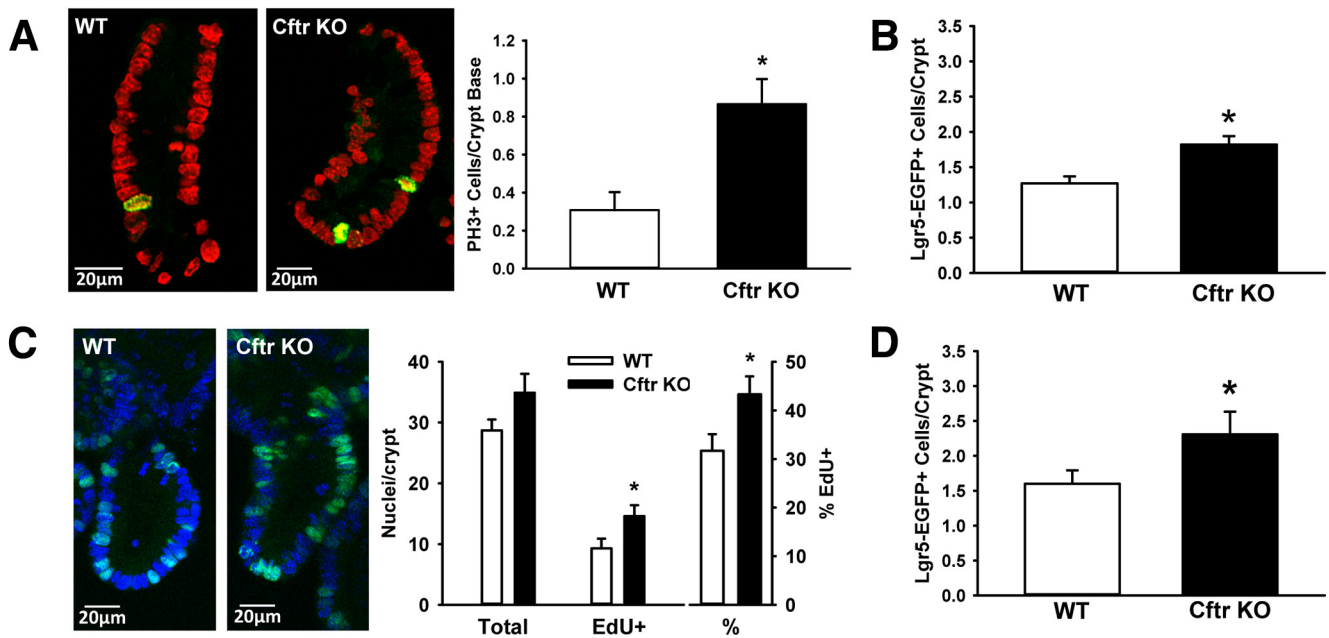


**Figure 1. Increased proliferation in the Cftr KO intestine ex vivo and early passage enteroids.** (A) *Left:* Isolated crypts from WT and Cftr KO mice labeled for PH3 (green), a marker of mitosis. Nuclei are labeled with TO-PRO 3 nuclear stain (red). *Right:* Cumulative data showing differences in proliferation rates between freshly isolated WT and Cftr KO crypts as measured by PH3 immunofluorescence. Data are expressed as the number of PH3+ cells/cryptbase optical cross-section. \* $P < .001$ ;  $n = 4$  WT/Cftr KO pairs (32–38 crypts/genotype). (B) Cumulative data showing the average Lgr5-EGFP+ stem cell numbers/Lgr5-EGFP+ crypt in freshly isolated crypts from WT/Lgr5-EGFP and Cftr KO/Lgr5-EGFP small intestine. \* $P < .02$ ;  $n = 3$  WT/Cftr KO pairs (81–113 Lgr5+ crypts/genotype). (C) *Left:* Enteroid crypts from WT and Cftr KO mice labeled with EdU for S-phase nuclei (green). Nuclei are labeled with 4',6-diamidino-2-phenylindole nuclear stain (blue). *Right:* Cumulative data showing differences in proliferation rates between WT and Cftr KO enteroid crypts as measured by EdU+ nuclei and the percentage of EdU+ (%EdU+ nuclei) per crypt optical cross-section. \* $P < .03$ ;  $n = 5$  WT/Cftr KO pairs (48–52 crypts/genotype). (D) Cumulative data showing the average Lgr5-EGFP+ stem cell numbers/Lgr5-EGFP+ crypt in enteroid crypts from WT and Cftr KO small intestine. \* $P < .05$ ;  $n = 5$  WT/Cftr KO pairs (156–171 Lgr5+ crypts/genotype).

31.7%  $\pm$  3.4% EdU+ of total crypt nuclei in early passages to 43%  $\pm$  4% EdU+ at passage 4 ( $P < .002$ ;  $n = 5$ –6). Cftr KO enteroids averaged 42%  $\pm$  4% EdU+ of total crypt nuclei in early passage and 43%  $\pm$  2% EdU+ at passage 4 (ns;  $n = 5$ ). Corresponding to the increased proliferation in the WT at passage 4, immunoblot analysis of passage 4 WT enteroids showed decreased protein expression of Cftr (-50.6% relative to passage 1;  $P < .02$ ;  $n = 4$ –6 WT mice). These findings are consistent with earlier studies of cell lines expressing human CFTR (hCFTR), which showed growth suppression upon functional hCFTR expression and improved proliferation in cells expressing dysfunctional CFTR.<sup>42,43</sup> We postulate that cells with low levels of CFTR activity have a growth advantage and dominate in subsequent generations, which apparently extends to successive passages of WT enteroid cultures.

#### Increased Wnt/ $\beta$ -Catenin Signaling in CFTR KO Intestinal Crypts Is Recapitulated in Early Passage Enteroids

Wnt/ $\beta$ -catenin signaling is required for the maintenance of the ISC population.<sup>28</sup> With evidence of increased proliferation in both freshly isolated Cftr KO crypts and enteroids, we asked whether Wnt/ $\beta$ -catenin signaling was associated

with increased proliferation in the Cftr KO intestine. Freshly isolated crypts and enteroids from the same WT and Cftr KO matched mice were compared by immunoblot analysis for levels of active  $\beta$ -catenin, defined as  $\beta$ -catenin dephosphorylated at Ser37 and Thr41,<sup>44</sup> and an immediate down-stream Wnt target gene, *Lef1*.<sup>45</sup> As a positive control for enhanced Wnt/ $\beta$ -catenin signaling, WT enteroids were treated with Wnt3a-conditioned medium for 24 hours before collection. The immunoblot shown in Figure 2A indicates that both freshly isolated crypts and enteroids from Cftr KO mice have greater levels of active  $\beta$ -catenin and *Lef1* compared with those from matched WT mice. Densitometric analysis showed statically significant increases in active  $\beta$ -catenin and *Lef1* in fresh crypts (Figure 2B) and in the enteroids (Figure 2C). These findings indicate that increased Wnt/ $\beta$ -catenin signaling may contribute to increased ISC proliferation in Cftr KO intestine in vivo and in early passage enteroids.

#### Cftr Expression and Function in WT Lgr5+ Intestinal Stem Cells

CFTR possesses an intestinal-specific enhancer element in intron 1 that is positively regulated by transcription factor 4, and is therefore a target of Wnt signaling.<sup>46</sup> Based

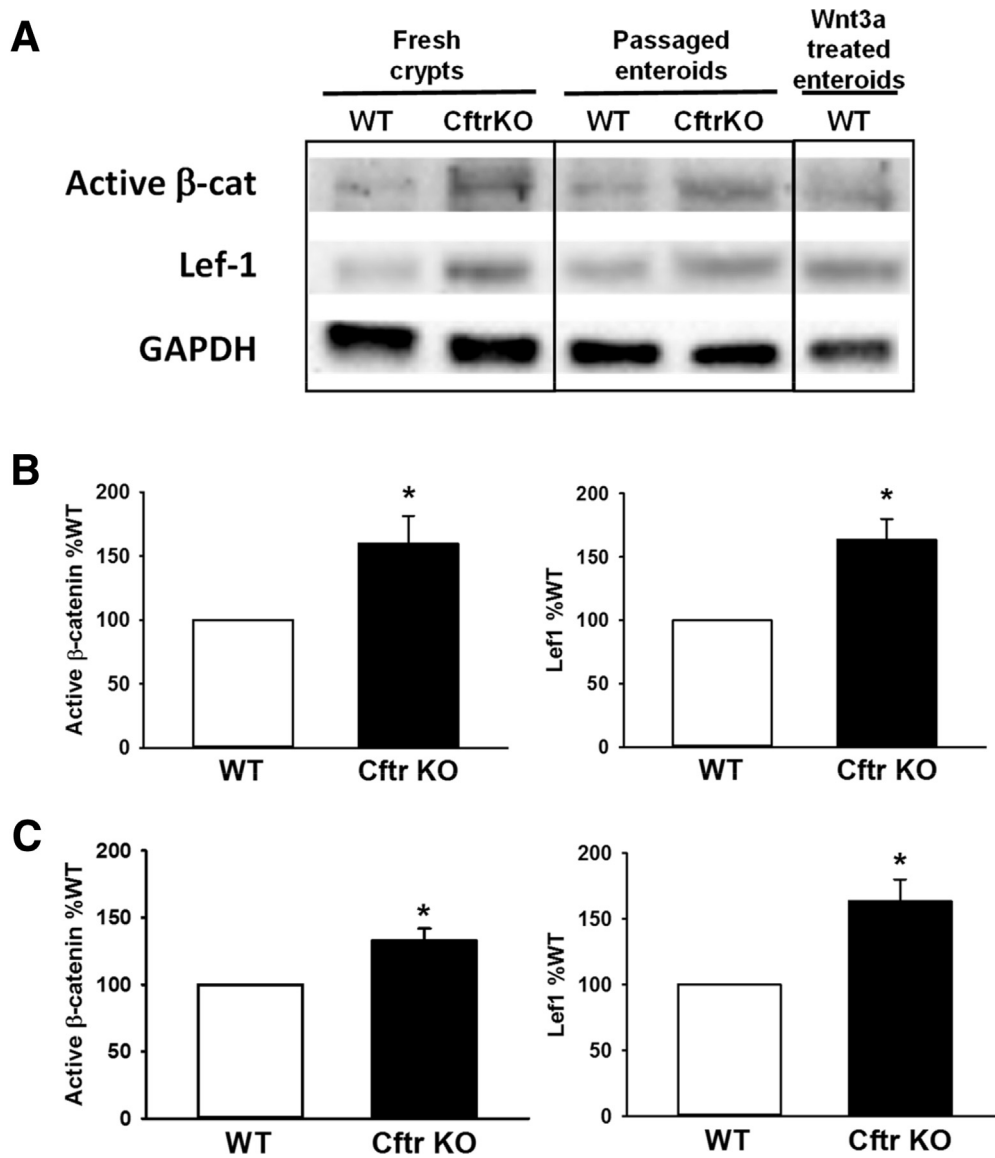


**Figure 2. Increased Wnt/ $\beta$ -catenin signaling in the Cftr KO intestine ex vivo and early passage enteroids.** (A) Immunoblot for active  $\beta$ -catenin (dephosphorylated at Ser37/Thr41) and downstream Wnt target gene Lef1 using freshly isolated crypts (Fresh crypts) and passage 1 enteroids (Passaged enteroids) from a matched pair of WT and Cftr KO mice. Right: WT enteroids treated with Wnt3a conditioned medium for 24 hours before collection. (B) Left: Densitometric analysis for immunoblots of active  $\beta$ -catenin from WT and Cftr KO freshly isolated crypts. Glyceraldehyde-3-phosphate dehydrogenase (GAPDH) or  $\beta$ -actin were used as loading controls. Data are presented as % WT;  $n = 11$  WT/Cftr KO pairs.  $*P < .03$ . Right: Densitometric analysis for immunoblots of Lef1 protein expression from WT and Cftr KO isolated crypts. GAPDH or  $\beta$ -actin were used as loading control. Data are presented as % WT;  $n = 7$  WT/Cftr KO pairs. (C) Left: Densitometric analysis for immunoblots of active  $\beta$ -catenin from WT and Cftr KO enteroids. GAPDH or  $\beta$ -actin were used as loading controls. Data are presented as % WT;  $n = 5$  WT/Cftr KO pairs.  $*P < .02$ . Right: Densitometric analysis for immunoblots of Lef1 protein expression in WT and Cftr KO enteroids. GAPDH or  $\beta$ -actin were used as loading controls. Data are presented as % WT;  $n = 4$  WT/Cftr KO pairs.  $*P < .03$ .

on finding increased Lgr5-EGFP<sup>+</sup> stem cell numbers in the Cftr KO intestine (Figure 1B and D) and evidence that CFTR functions as a growth suppressant/tumor suppressor,<sup>13,42,43</sup> we asked whether Cftr is expressed and active in ISCs. Different expression levels of SOX9 transcription factor modulate intestinal stem cell proliferation and serve as a marker of crypt cell type.<sup>36</sup> Fluorescence-activated cell sorting of intestinal epithelium from Sox9<sup>EGFP</sup> transgenic mice have shown that low-expressing Sox9<sup>EGFP</sup> (Sox9<sup>EGFPLo</sup>)

cells are CBCs that are enriched in Lgr5 and form enteroids in culture.<sup>36,47</sup> Therefore, intestinal epithelial cells from Sox9<sup>EGFP</sup> mice were sorted into expression fractions and immunoblotted for Cftr. As shown by the immunoblot in Figure 3A, the Sox9<sup>EGFPLo</sup> cell fraction had a significant amount of Cftr relative to the Sox9<sup>EGFPSubLo</sup> fraction, representing transit-amplifying progenitor cells, and the Sox9<sup>EGFPNeg</sup> fraction, representing the differentiated cell types including enterocytes, goblet cells, and Paneth cells.

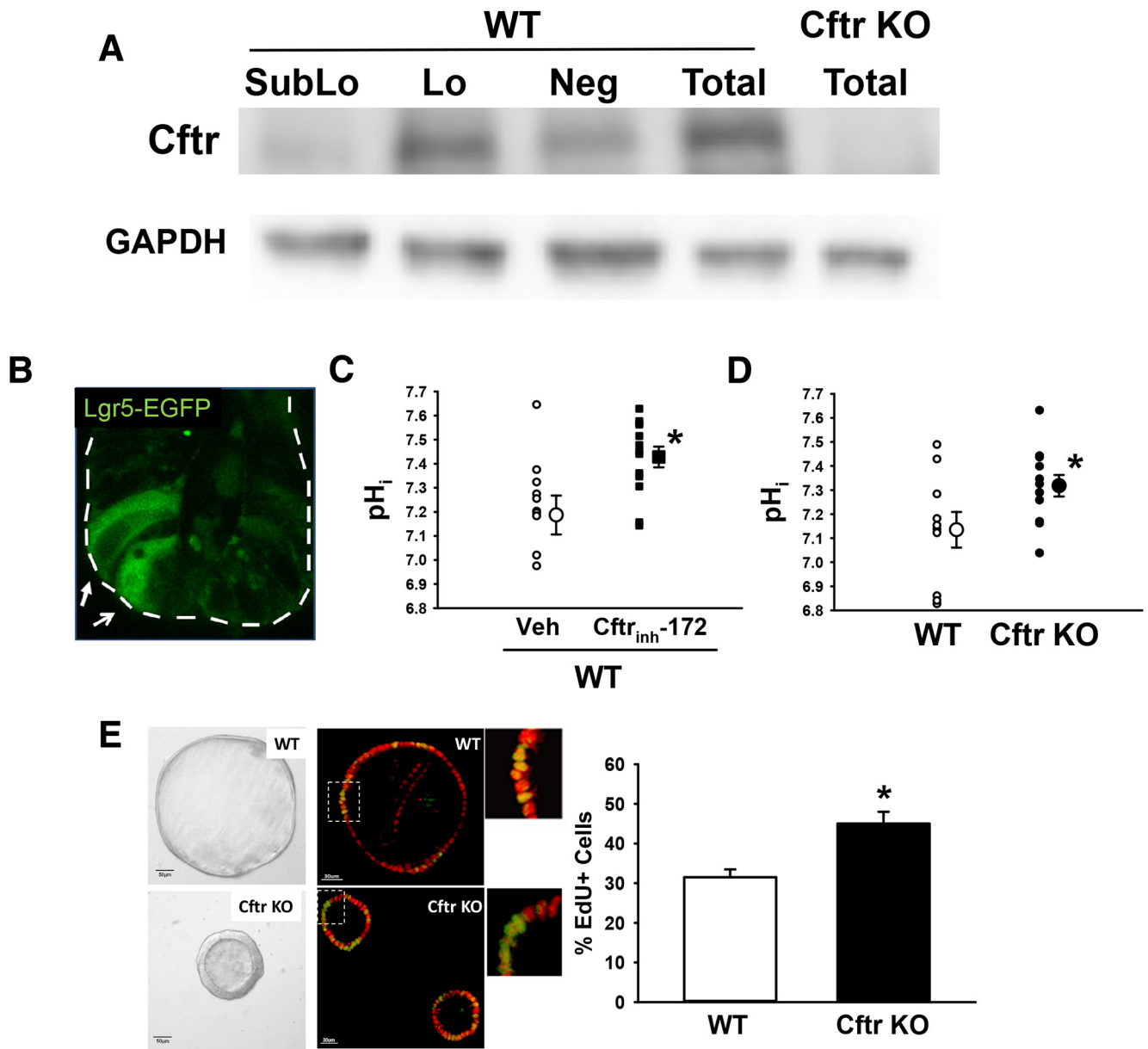


**Figure 3. Expression and function of Cftr in small intestinal stem cells.** (A) Immunoblot for Cftr in flow cytometry cell fractions of small intestinal epithelium isolated from Sox9<sup>EGFP</sup> mice. SubLo, sublow Sox9<sup>EGFP</sup>-expressing cell fraction (transit-amplifying progenitors); Lo, low Sox9<sup>EGFP</sup>-expressing cell fraction (crypt-base stem cells, Lgr5+); Neg, negative for Sox9<sup>EGFP</sup> expression cell fraction (enterocyte, goblet, Paneth); Total, total small intestinal epithelium. Cftr KO total epithelium, negative control. Glyceraldehyde-3-phosphate dehydrogenase (GAPDH), loading control. Representative of 3 Sox9<sup>EGFP</sup> mice. (B) Confocal micrograph of Lgr5-EGFP-expressing intestinal stem cells in crypt epithelium (white arrows). White dashed line outlines crypt. (C) Intracellular pH of Lgr5-EGFP+ cells in WT/Lgr5-EGFP enteroids treated with either dimethyl sulfoxide (vehicle, small circles) or Cftr<sub>inh</sub>-172 (10 μmol/L for 1 h, large squares). Treatment average, large circle or square. \*P < .02 vs vehicle; n = 10–13 Lgr5-EGFP cells from 7–8 enteroids cultured from 6 WT/Lgr5-EGFP mice. (D) Intracellular pH of Lgr5-EGFP+ cells in enteroids from matched WT/Lgr5-EGFP (open small circles) and Cftr KO/Lgr5-EGFP (filled small circles) mice. Average shown as large circles. \*P < .04; n = 10–12 Lgr5-EGFP cells from 6 enteroids from 3 WT/Lgr5-EGFP and Cftr KO/Lgr5-EGFP matched mice. (E) Left: ISC-enriched enterospheres from WT and Cftr KO matched mice and a photomicrograph showing EdU-positive nuclei (green) and nuclei (red) in an optical cross-section of WT and Cftr KO enterospheres. Right: Percentage of EdU-positive nuclei relative to total nuclei in optical cross-sections of WT and Cftr KO enterospheres. (Total number of nuclei/enterosphere was WT = 36.1 ± 3.8; Cftr KO = 46.7 ± 2.0, n = 32 enterospheres/genotype; P < .009). \*P < .05 vs WT; n = 4 WT and Cftr KO matched mice (8 enterospheres/mouse).

To investigate Cftr functional activity in ISCs, we examined the effect of Cftr inhibition or ablation on the  $pH_i$  of Lgr5-EGFP+ stem cells using enteroids from matched WT/Lgr5-EGFP and Cftr KO/Lgr5-EGFP mice. Previous studies have shown that acute inhibition of Cftr using the channel blocker Cftr<sub>inh</sub>-172 alkalizes  $pH_i$  in the crypt epithelium of WT enteroids.<sup>19</sup> More importantly,  $pH_i$  of crypt epithelium in Cftr KO enteroids is uncompensated and maintains an alkaline  $pH_i$ ,<sup>19,20</sup> similar to reports of duodenal villous epithelium from Cftr KO mice<sup>37,48</sup> and cystic fibrosis pancreatic adenocarcinoma cells, a pancreatic cell line derived from a CF patient.<sup>49</sup> To measure intracellular pH in Lgr5-EGFP+ stem cells (Figure 3B), enteroids were loaded with the ratiometric, pH-sensitive dye SNARF-5F for confocal microfluorimetry. As shown in Figure 3C, the  $pH_i$  in WT Lgr5-EGFP stem cells significantly increased by ~0.2 pH units after a 1-hour treatment with Cftr<sub>inh</sub>-172 (10  $\mu$ mol/L). Moreover, as shown in Figure 3D, Cftr KO Lgr5-EGFP+ stem cells show an alkaline  $pH_i$  that is also ~0.2 pH units greater than in WT Lgr5-EGFP+ stem cells. These findings indicate that both acute and chronic loss of Cftr function alkalizes Lgr5-EGFP+ intestinal stem cells, indicative of a  $pH_i$  regulatory role by Cftr anion channel activity in WT ISCs.

Primary culture of dissociated small intestinal crypt epithelium with exogenous Wnt3a (100 ng/mL) results in the formation of ISC-enriched epithelial spheroids (enterospheres).<sup>50–54</sup> In examining Cftr stem cell activity, we asked whether ISC-enriched enterospheres from WT and Cftr KO would show differences in proliferation consistent with our study enumerating Lgr5-EGFP+ ISCs/crypt (Figure 1B and D). As shown in Figure 3E (left), WT enterospheres formed enlarging monolayer cysts, suggesting Cftr-mediated fluid secretion. In contrast, Cftr KO enterospheres had much smaller luminal cavities and slow cyst expansion with time in culture, as noted previously in studies of human CF colon organoids.<sup>55</sup> EdU and confocal optical cross-section studies were used to examine proliferation rates in WT and Cftr KO enterospheres. As shown in Figure 3E (right), Cftr KO enterospheres had a 38% greater rate of proliferation relative to WT enterospheres. These findings show a role of Cftr as a growth suppressant in an enriched ISC population.

### Intracellular Alkalinity and Membrane Association of Dvl2-EGFP in Cftr KO Crypt-Base Columnar Cells

Different facets of Wnt signaling play major roles in cellular processes of proliferation, cell migration, and polarity.<sup>27</sup> The signaling mediator Dvl is critical for downstream activation of both canonical and noncanonical Wnt signaling pathways through its recruitment to Fz membrane receptors.<sup>56</sup> The formation of a stable Dvl-Fz association involves both the binding of the PDZ domain of Dvl to the PDZ binding domain of Fz and the binding of the polybasic DEP domain of Dvl to negatively charged phosphatidic acid and phosphatidylglycerol at the inner leaflet of the plasma membrane.<sup>26,57</sup> The latter process is both charge- and  $pH_i$ -dependent, wherein a more alkaline  $pH_i$  facilitates

electrostatic attraction of the polybasic DEP domain to the cell membrane. Importantly, the 3 major domains of Dvl are conserved across species, including the PDZ and DEP domains.<sup>27</sup> Based on evidence of alkalinity and increased proliferation in Cftr KO ISCs, we asked whether Dvl in Cftr KO CBCs associates more closely with the plasma membrane as a means to facilitate Wnt/ $\beta$ -catenin signaling.

Subcellular localization of the major Dvl isoform in mice, Dvl2, was imaged by confocal microscopy in live WT and Cftr KO enteroids from transgenic mice that express Dvl2-EGFP (native Dvl2 KO) and the Rosa<sup>MT/mG</sup> plasma membrane reporter (Figure 4A). Measurements of Dvl2-EGFP proximity to the cell membrane were limited to the supranuclear region (ie, between the apical pole of the nucleus and the apical membrane), owing to the close apposition of the nucleus/nuclear membrane to the plasma membrane in the basal portion of the cell. To evaluate whether  $pH_i$  differences between WT/Dvl2-EGFP/Rosa<sup>MT/mG</sup> and Cftr KO/Dvl2-EGFP/Rosa<sup>MT/mG</sup> CBC cells were present in this cell region, high-resolution SNARF-5F confocal microfluorimetry measured  $pH_i$  in the supranuclear region of nongranulated CBC cells, serving as proxy for Lgr5+ ISCs.<sup>30</sup> As shown in Figure 4B, Cftr KO enteroids showed a significantly more alkaline  $pH_i$  in the supranuclear region of CBCs as compared with WT, therefore confirming  $pH_i$  differences in this region. As depicted in the model shown in Figure 4C, the membrane proximity of Dvl2-EGFP to the supranuclear lateral membrane of a CBC was measured as the EGFP intensity within a 2-pixel distance (1.15  $\mu$ m) interior to the lateral and medial mTomato plasma membranes (relative to crypt axis) from the apical pole of the nucleus to the apical membrane. As shown in Figure 4D (left), the Cftr KO CBCs showed greater juxtamembrane Dvl2-EGFP intensity at the supranuclear lateral plasma membranes than was found in WT CBCs. Interestingly, as shown in Figure 4D (right), the WT CBCs showed a polarized distribution of Dvl2-EGFP with significantly greater juxtamembrane Dvl2-EGFP intensity at the lateral-Lateral membrane than at the medial-Lateral cell membrane. The juxtamembrane Dvl2-EGFP intensity at the medial-Lateral membrane was not different from the average EGFP intensity of all supranuclear pixels (ie, no detectable association). In contrast, the juxtamembrane Dvl2-EGFP intensity at the lateral-Lateral membrane in the Cftr KO CBCs was similar to that of WT but significantly greater than WT at the medial-Lateral membrane, indicating a less polarized distribution of Dvl2 at the lateral plasma membrane in Cftr KO CBCs.

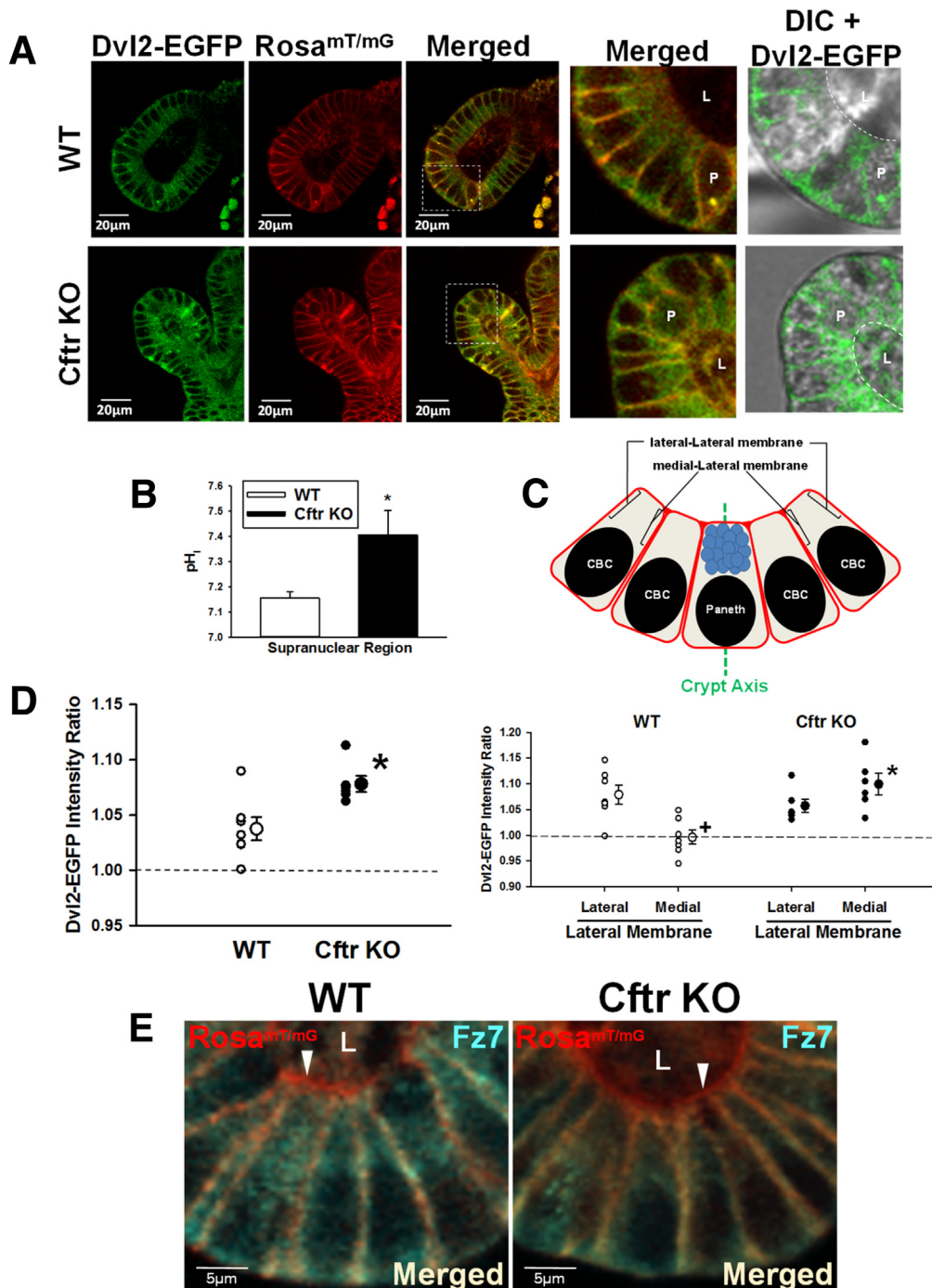
The Dvl2-EGFP intensity ratio shown in Figure 4D is the averages of WT and Cftr KO matched mice. In the analysis, we found the Dvl2-EGFP intensity ratio between individual enteroid crypts (consisting of the average of 1–3 CBCs/crypt) showed greater variability than between individual mice of the same genotype. However, the average Dvl2-EGFP intensity ratio at the lateral cell membranes of WT and Cftr KO crypts was nearly identical to the per-mouse averages shown in Figure 4D, right (WT =  $1.04 \pm 0.01$  vs Cftr KO =  $1.08 \pm 0.01$  intensity ratio,  $n = 18$  and  $13$  crypts, respectively;  $P < .02$ ). Thus, enteroid crypt averages from paired WT-Cftr KO mice also provide a robust comparison of the juxtamembrane Dvl2-EGFP intensity ratio between the 2 genotypes.

To determine whether increased localization of Dvl2 at the supranuclear lateral plasma membrane was positioned to facilitate Wnt/ $\beta$ -catenin signaling, immunofluorescence studies evaluated the plasma membrane localization of the primary Wnt receptor for canonical Wnt/ $\beta$ -catenin signaling in ISC (ie, Fz7).<sup>58</sup> As shown in Figure 4E, the distribution of Fz7 appeared uniform along the entire lateral plasma membrane of CBC cells in both WT and Cftr KO enteroids. Fz7 was not localized to the apical (lumen-facing) membrane of CBCs. Thus, the supranuclear region of live CBCs is

appropriate for evaluating Dvl2-EGFP membrane association and its potential for facilitating Wnt/ $\beta$ -catenin signaling in WT and Cftr KO enteroids.

*Neutralization of Plasma Membrane Charge in Cftr KO Enteroids Reduces Dvl2 Proximity to the Plasma Membrane*

The DEP domain of Dvl binds to acidic lipid headgroups of phosphatidic acid and phosphatidylglycerol at physiological



pH.<sup>26</sup> In HEK293T cells, neutralization of negatively charged phospholipids with the cationic lipid sphingosine reduced Dvl-Fz association by interfering with the electrostatic interaction of the Dvl DEP domain with the inner leaflet of the plasma membrane.<sup>26</sup> To examine the effect of neutralizing the negatively charged inner leaflet phospholipids in Cftr KO CBCs, Dvl2-EGFP intensity at the supranuclear plasma membrane was measured in Cftr KO enteroids treated for 1 hour with 75  $\mu\text{mol/L}$  sphingosine or vehicle (Figure 5A, left). As shown in Figure 5A (right), Dvl2-EGFP intensity at the CBC supranuclear plasma membrane was significantly reduced in sphingosine-treated enteroids compared with vehicle control. Sphingosine significantly reduced Dvl2-EGFP membrane association at both the lateral-Lateral and medial-Lateral cell membranes of the Cftr KO CBCs (vehicle lateral-Lateral =  $1.09 \pm 0.02$  and medial-Lateral =  $1.10 \pm 0.01$  vs sphingosine lateral-Lateral =  $0.92 \pm 0.02$  vs medial-Lateral =  $0.97 \pm 0.01$  intensity ratio; vs vehicle lateral-Lateral membrane;  $P < .001$ ; vs vehicle medial-Lateral membrane;  $P < .001$ ). A comparison of enteroid crypt averages for vehicle and sphingosine treatments yielded similar results (vehicle =  $1.10 \pm 0.01$  vs sphingosine =  $0.95 \pm 0.01$  intensity ratio;  $n = 11$  crypts each;  $P < .000000001$ ). Prolonged sphingosine treatment (2–3 h) proved toxic in that enteroids began to dissociate with cell rounding, therefore, we did not attempt to measure active  $\beta$ -catenin protein under this condition. Nonetheless, the earlier-described findings indicate that Dvl2 association with the plasma membrane is charge-dependent in Cftr KO CBC cells.

### Reduction of pH<sub>i</sub> in Cftr KO Enteroid CBCs Reduces Dvl2 Plasma Membrane Association

Alkalinity reduces proton interaction with the negatively charged domains of membrane phospholipids, allowing for greater interaction with the Dvl2-DEP domain.<sup>26,59</sup> Therefore, the pH<sub>i</sub> in Cftr KO enteroid crypts was manipulated by

culturing Cftr KO/Dvl2-EGFP/Rosa<sup>mT/mG</sup> enteroids for 3 days in pH 7.1 medium followed by 2 days in medium at either pH 6.6 or maintained in pH 7.1 medium (controls). In the pH 6.6 medium, the pH<sub>i</sub> was reduced by  $-0.31 \pm 0.06$  pH units relative to pH 7.1 medium ( $P < .0002$ ;  $n = 13$  CBC from 2–4 enteroids from 3 Cftr KO mice). Overt cell/enteroid morphology was unaffected by pH 6.6 medium (Figure 5B, left). Cftr KO enteroids cultured in pH 6.6 medium, as compared with pH 7.1 medium, showed reduced Dvl2-EGFP intensity at the supranuclear lateral plasma membranes of CBCs (Figure 5B, right). Both the lateral-Lateral and medial-Lateral membranes showed reduced Dvl2-EGFP intensity in the acidified Cftr KO CBCs (pH 7.1: lateral-Lateral =  $1.08 \pm 0.01$  and medial-Lateral =  $1.10 \pm 0.01$ ; pH 6.6: lateral-Lateral =  $1.00 \pm 0.03$  vs medial-Lateral =  $1.00 \pm 0.03$  intensity ratio;  $P < .03$  and  $P < .01$ , respectively). Similar results were yielded by comparison of crypt averages for the 2 conditions (pH 7.1 =  $1.09 \pm 0.01$  vs pH 6.6 =  $0.99 \pm 0.01$  intensity ratio;  $n = 11$  and 7 crypts, respectively;  $P < .00000002$ ). Measurements of Cftr KO enteroids exposed to the pH 6.6 medium showed a significantly reduced active  $\beta$ -catenin compared with pH 7.1 medium (as the percentage of pH 7.1 [100%]: pH 6.6 =  $64.9\% \pm 5.1\%$ ;  $P < .03$ ; enteroids from  $n = 5$  Cftr KO mice). Acidic conditions influence cell proliferation in several ways<sup>60</sup>; therefore, proliferation of Cftr KO enteroids maintained in pH 6.6 medium was not investigated.

### Acute Pharmacologic Manipulation of Dvl2-EGFP Plasma Membrane Association in CBCs

Recent studies have shown that the alkaline pH<sub>i</sub> of crypt epithelium in Cftr KO enteroids can be acutely reduced by pharmacologic reduction of intracellular [Cl<sup>-</sup>], which facilitates basolateral anion exchanger 2 normalization of pH<sub>i</sub>.<sup>20</sup> To further assess the relationship between pH<sub>i</sub> and

**Figure 4. (See previous page). Increased Dvl2-EGFP localization at the plasma membrane in Cftr KO crypt-base columnar cells.** (A) Representative images of WT/Dvl2-EGFP/Rosa<sup>mT/mG</sup> (top) and Cftr KO/Dvl2-EGFP/Rosa<sup>mT/mG</sup> (bottom) enteroid crypts showing Dvl2-EGFP (green), Rosa<sup>mT/mG</sup> (red), and merged images. Magnified merged and differential interference contrast merged with Dvl2-EGFP (DIC+Dvl2-EGFP) images of crypt base (from white boxes), were magnified ( $\times 3.6$ ). P, Paneth cell; L, crypt lumen. White dashed lines outline apical membrane orient toward the crypt lumen. (B) Cumulative pH<sub>i</sub> data for the supranuclear region of CBCs in WT and Cftr KO enteroids.  $*P < .03$  vs WT;  $n = 4$ –8 crypts from 4 WT and Cftr KO matched mice. (C) Crypt base model depicting the measurement by confocal microfluorimetry of Dvl2-EGFP intensity 2 pixels interior to the lateral-Lateral Membrane (lateral to central crypt axis) and medial-Lateral membrane (medial to central crypt axis) plasma membrane of CBCs. Green dashed line, central crypt axis. Brackets indicate sites of measurement on the supranuclear lateral plasma membranes. Paneth, Paneth cell. (D) Left: Cumulative data showing the average Dvl2-EGFP intensity ratio within 1.15  $\mu\text{m}$  of the CBC supranuclear plasma membrane of individual mice (small circles) and overall average (large circles) for WT/Dvl2-EGFP/Rosa<sup>mT/mG</sup> (WT) and Cftr KO/Dvl2-EGFP/Rosa<sup>mT/mG</sup> (Cftr KO) sex-matched mouse pairs ( $n = 7$  and 6 mice, respectively). Dashed line indicates the average Dvl2-EGFP pixel intensity for the entire supranuclear region of CBC, which has been set to 1.0 (average intensity =  $59.5 \pm 8.8$  for WT and  $88.5 \pm 15.9$  for Cftr KO; ns;  $n = 7$ –6 mice, respectively; average of 1–3 CBCs/crypt from 2 to 4 crypts of passage 1 and 2 enteroids).  $*P < .01$  vs WT plasma membrane. Right: Cumulative data showing the average Dvl2-EGFP intensity ratio at the individual supranuclear lateral-Lateral and medial-Lateral plasma membranes of individual mice (small circles) and overall average (large circles) for WT/Dvl2-EGFP/Rosa<sup>mT/mG</sup> (WT) and Cftr KO/Dvl2-EGFP/Rosa<sup>mT/mG</sup> (Cftr KO) sex-matched mouse pairs ( $n = 7$  and 6 mice, respectively). Dashed line indicates the average Dvl2-EGFP pixel intensity for the entire supranuclear region of CBC, which has been set to 1.0.  $^+P < .002$  vs WT lateral-Lateral cell membrane;  $*P < .001$  vs WT medial-Lateral cell membrane. (E) Immunofluorescence image of Fz7 (cyan), plasma membrane (red), and merged (light yellow) of CBCs in WT and Cftr KO enteroid crypts. Representative of 3 WT-Cftr KO mouse pairs. L, lumen. White arrowheads denote lack of Fz7 staining at apical membrane (red).

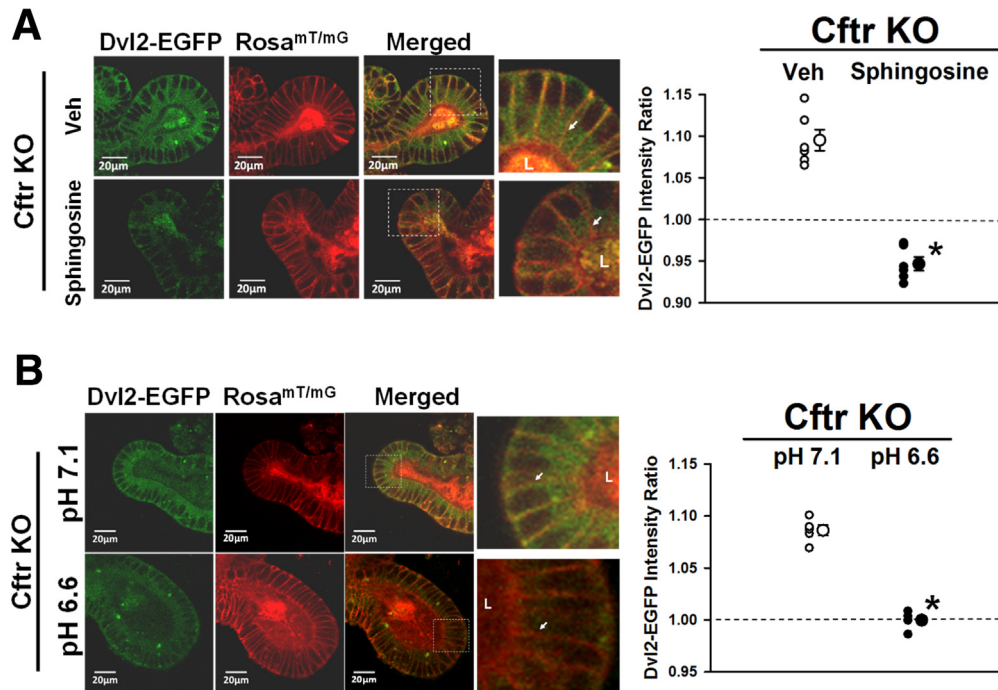


**Figure 5. Dvl2-EGFP proximity to the plasma membrane is charge- and pH<sub>i</sub>-dependent in Cfr KO crypt-base columnar cells.** (A) *Left:* Representative images of ETOH vehicle- (Veh, *top*) and sphingosine-treated (Sphingosine, *bottom*) Cfr KO/Dvl2-EGFP/Rosa<sup>mT/mG</sup> enteroid crypts showing Dvl2-EGFP (green), Rosa<sup>mT/mG</sup> (red), and merged images. Magnified merged image ( $\times 2.5$ ) of crypt base (from *white boxes*). L, crypt lumen; lateral cell membrane for comparison (*white arrows*). *Right:* Cumulative data showing the average Dvl2-EGFP intensity ratio within 1.15  $\mu\text{m}$  of the CBC supranuclear plasma membrane of individual mice (*small circles*) and overall average (*large circles*) for vehicle- and sphingosine-treated Cfr KO/Dvl2-EGFP/Rosa<sup>mT/mG</sup> (Cfr KO) mice ( $n = 6$ ). *Dashed line* indicates the average Dvl2-EGFP pixel intensity for the entire supranuclear region of CBC, which has been set to 1.0.  $*P < .001$  vs vehicle. Averaged data for each mouse represents measurements from 1 to 3 CBCs/crypt from 2 to 4 crypts from passage 1 and 2 enteroids. (B) *Left:* Representative images of Cfr KO enteroids cultured for 48 hours in medium, pH 7.1 (*top*), and medium, pH 6.6 (*bottom*), showing Dvl2-EGFP (green), Rosa<sup>mT/mG</sup> (red), and merged images. Magnified merged image ( $\times 4.1$ ) of crypt base (from *white boxes*). L, crypt lumen; lateral cell membrane for comparison (*white arrows*). *Right:* Cumulative data showing the average Dvl2-EGFP intensity ratio within 1.15  $\mu\text{m}$  of the CBC supranuclear plasma membrane of individual mice (*small circles*) and overall average (*large circles*) for pH 7.1- and pH 6.6-treated enteroids from Cfr KO/Dvl2-EGFP/Rosa<sup>mT/mG</sup> (Cfr KO) mice ( $n = 4$ ). *Dashed line* indicates the average Dvl2-EGFP pixel intensity for the entire supranuclear region of CBC, which has been set to 1.0.  $*P < .001$  vs pH 7.1 medium. Averaged data for each mouse represents measurements from 1 to 3 CBCs/crypt from 2 to 4 crypt from passage 1 and 2 enteroids.

Dvl2-EGFP membrane association, Cfr KO/Dvl2-EGFP/Rosa<sup>mT/mG</sup> enteroids were treated for 30 minutes with a sequential combination of 50  $\mu\text{mol/L}$  bumetanide (15 min) to inhibit Cl<sup>-</sup> uptake by the NKCC1, followed by 100  $\mu\text{mol/L}$  carbachol (15 min) to induce epithelial Cl<sup>-</sup> secretion by Ca<sup>2+</sup>-activated Cl<sup>-</sup> channels (eg, Ano1). As shown in Figure 6A, pharmacologic treatment to normalize pH<sub>i</sub> by reducing intracellular Cl<sup>-</sup> concentration significantly reduced Dvl2-EGFP association at the supranuclear lateral plasma membranes in Cfr KO CBCs. Both the lateral-Lateral and medial-Lateral membranes had significantly reduced Dvl2-EGFP membrane association in the treated Cfr KO CBCs (vehicle: lateral-Lateral =  $1.08 \pm 0.02$  and medial-Lateral =  $1.10 \pm 0.02$ ; Bumet-CCH: lateral-Lateral =  $0.97 \pm 0.04$  vs medial-Lateral =  $1.02 \pm 0.01$  intensity ratio;  $P < .03$  and  $P < .03$ ; respectively). In a converse experiment, WT enteroids were treated with a combination of 10  $\mu\text{mol/L}$  Cfr<sub>inh</sub>-172 and 20  $\mu\text{mol/L}$  GlyH-101 for 1 hour to inhibit Cfr

Cl<sup>-</sup> and HCO<sub>3</sub><sup>-</sup> conductance at both extracellular and intracellular sites, respectively.<sup>61</sup> As shown in Figure 6B, pharmacologic inhibition of Cfr to increase WT ISC pH<sub>i</sub> significantly increased Dvl2-EGFP association with the supranuclear lateral cell plasma membrane to a level similar to Cfr KO CBCs (Figure 4D). The increase in Dvl2-EGFP membrane association primarily occurred at the medial-Lateral plasma membrane in the WT enteroids treated with Cfr inhibitors (vehicle: lateral-Lateral =  $1.05 \pm 0.03$  and medial-Lateral =  $1.02 \pm 0.01$ ; Cfr inhibitors lateral-Lateral =  $1.09 \pm 0.01$  and medial-Lateral =  $1.10 \pm 0.01$  intensity ratio; ns and  $P < .0005$ , respectively). Both of the earlier-described studies were paralleled by crypt averages for the 2 experiments (vehicle =  $1.09 \pm 0.01$  vs Bumet-CCH =  $0.99 \pm 0.02$  intensity ratio;  $n = 6$  and 8 crypts, respectively;  $P < .003$ ; vehicle =  $1.03 \pm 0.01$  vs Cfr<sub>inh</sub>-172-GlyH 101 =  $1.09 \pm 0.01$  intensity ratio;  $n = 6$  crypts each;  $P < .009$ ). Because both manipulations of pH<sub>i</sub> were acute, it

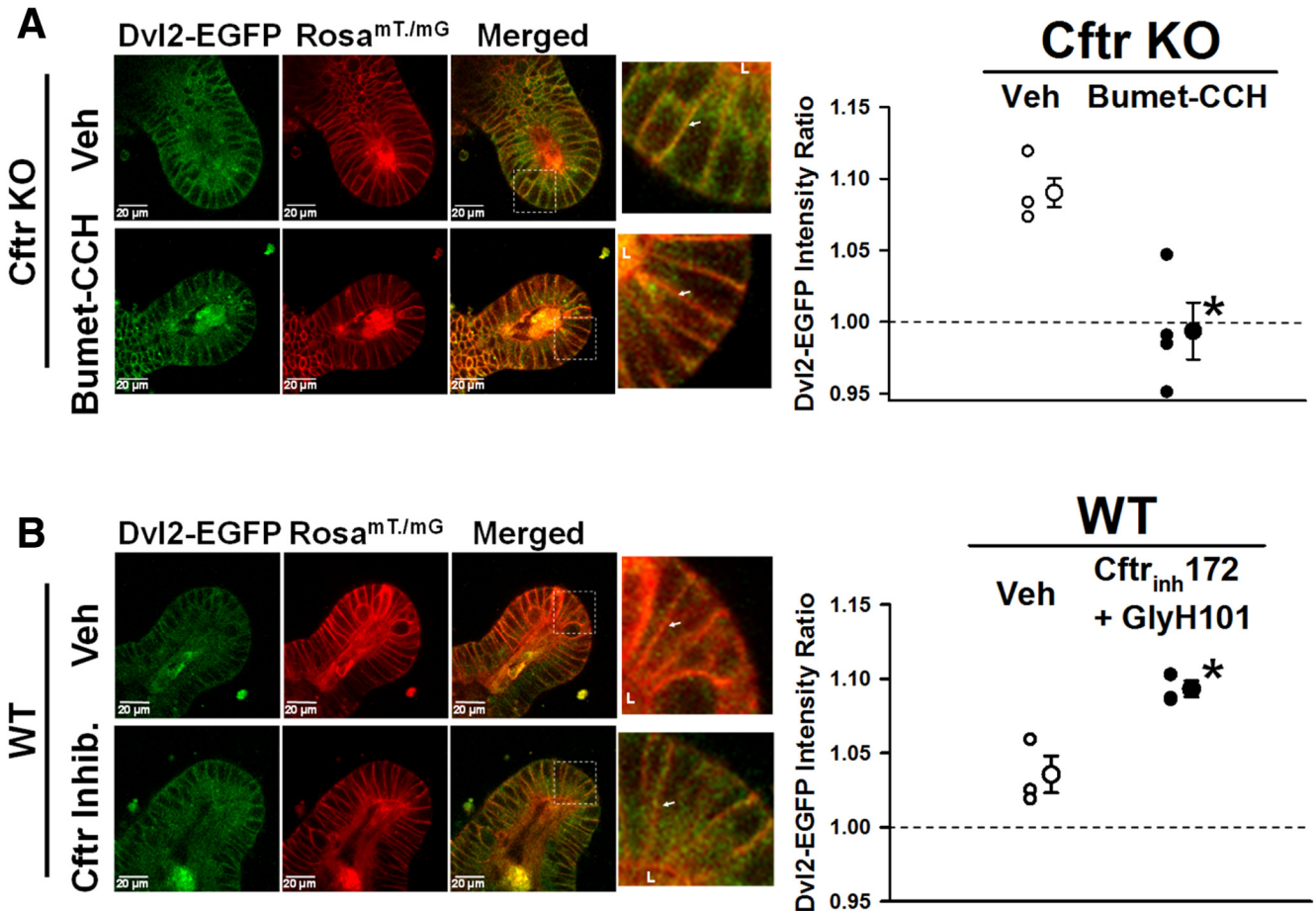


**Figure 6. Pharmacologic manipulation of Dvl2-EGFP plasma membrane association.** (A) *Left:* Representative images of dimethyl sulfoxide vehicle- (Veh, top) and bumetanide + carbachol-treated (Bumet-CCH, bottom) Cfr KO/Dvl2-EGFP/Rosa<sup>MT/mG</sup> enteroid crypts showing Dvl2-EGFP (green), Rosa<sup>MT/mG</sup> (red), and merged images. Magnified merged image ( $\times 3.6$ ) of crypt base (from white boxes). L, crypt lumen; lateral cell membrane for comparison (white arrows). *Right:* Cumulative data showing the average Dvl2-EGFP intensity ratio within  $1.15 \mu\text{m}$  of the CBC supranuclear lateral plasma membrane of individual mice (small circles) and overall average (large circles). Cfr KO/Dvl2-EGFP/Rosa<sup>MT/mG</sup> (Cfr KO) mice were treated with vehicle (Veh, dimethyl sulfoxide) or sequential exposure to  $50 \mu\text{mol/L}$  bumetanide (Bumet, 15 min) followed by  $100 \mu\text{mol/L}$  CCH (15 min),  $n = 4$  mice. Averaged data for each mouse represents measurements from 1 to 3 CBCs/crypt from 1 to 3 crypts from passage 1 and 2 enteroids. Dashed line indicates the average Dvl2-EGFP pixel intensity for the entire supranuclear region of CBC, which has been set to 1.0.  $*P < .005$  vs vehicle. (B) *Left:* Representative images of dimethyl sulfoxide vehicle- (Veh, top) and Cfr<sup>inh</sup>-172+GlyH-101-treated (Cfr Inhib., bottom) WT/Dvl2-EGFP/Rosa<sup>MT/mG</sup> enteroid crypts showing Dvl2-EGFP (green), Rosa<sup>MT/mG</sup> (red), and merged images. Magnified merged image ( $\times 3.8$ ) of crypt base (from white boxes). L, crypt lumen; lateral cell membrane for comparison (white arrows). *Right:* Cumulative data showing the average Dvl2-EGFP intensity ratio within  $1.15 \mu\text{m}$  of the CBC supranuclear lateral plasma membrane of individual mice (small circles) and overall average (large circles). WT/Dvl2-EGFP/Rosa<sup>MT/mG</sup> (WT) mice were treated with vehicle (Veh, dimethyl sulfoxide) or  $10 \mu\text{mol/L}$  Cfr<sup>inh</sup>-172 plus  $20 \mu\text{mol/L}$  GlyH-101 for 1 hour,  $n = 3$  mice. Averaged data for each mouse represents measurements from 1 to 3 CBCs/crypt from 2 to 4 crypts from passage 1 and 2 enteroids. Dashed line indicates the average Dvl2-EGFP pixel intensity for the entire supranuclear region of CBC, which has been set to 1.0.  $*P < .013$  vs vehicle.

was not expected that downstream accumulation of active  $\beta$ -catenin would be sufficient to warrant measurement.

## Discussion

Increased proliferation of the stem cell compartment is a potential risk factor for intestinal cancer.<sup>15</sup> Approximately 3 mutations occur with every division of a normal stem cell, therefore augmented stem cell proliferation raises the potential for a DNA replication error leading to “driver”

cancer mutations.<sup>16</sup> Cancer genome sequencing and epidemiologic studies suggest that stochastic DNA replication errors are responsible for two thirds of the mutations in human cancers.<sup>15,16</sup> One of the less commonly recognized manifestations of cystic fibrosis intestinal disease is an increased risk for gastrointestinal cancer. Previous studies have shown that CF patients have a 6- to 10-fold increased risk for GI cancer, which is surprising for a relatively young population, whereas the risk of non-digestive tract cancers in CF patients is similar to the general population.<sup>9,62</sup> The

risk of gastrointestinal cancer increases to 20-fold in patients ages 20–29 years and includes a significantly greater number of small intestinal tumors than in the non-CF population.<sup>9</sup> In accordance with increased GI cancer risk in CF patients, a recent study provided evidence that CFTR is a tumor-suppressor gene in human intestinal cancer.<sup>13</sup> The same study also showed a strong propensity of CF mice for spontaneous development of intestinal tumors when aged to 1 year with a penetrance of 60% compared with 0% in WT mice. The majority of tumors in CF mice were in the small intestine. One factor to consider here is that stem cell proliferation in the human colon exceeds that in the small bowel, whereas the inverse apparently holds true for mice.<sup>15</sup> Another factor deserving consideration is the propensity for intestinal cancer vs other cell/organ types in CF, which is not the case with many tumor-suppressor mutations or knockout models.<sup>63</sup> The diurnal and postprandial activity of Cftr in the alimentary tract is dynamic, which likely accentuates its role in pH<sub>i</sub> regulation and thus Wnt/ $\beta$ -catenin signaling in these epithelia. Unlike familial adenomatous polyposis or Lynch syndrome, which carry greater intestinal cancer risk owing to mutations directly involved in  $\beta$ -catenin signaling or DNA mismatch repair,<sup>64,65</sup> Cftr's role in growth suppression as outlined in this study is indirect and subject to known compensatory forces in the regulation of pH<sub>i</sub>.<sup>20</sup> Therefore, the propensity for gastrointestinal cancer in CF likely involves the combination of a life-long increase in ISC proliferation and the CF intestinal environment, which presents additional cancer risk factors including low-grade inflammation,<sup>4,5,11</sup> small-bowel bacterial overgrowth,<sup>3,12</sup> dysbiosis,<sup>66–68</sup> and goblet cell metaplasia.<sup>69</sup> With advances in CF respiratory therapy leading to increased life expectancy and the current prevalence of lung transplantation in CF patients,<sup>8</sup> there is a need to better understand the causes of intestinal hyperproliferation in the adult CF intestine and its relationship with cancer incidence.

Increased ISC proliferation in the Cftr KO intestine was maintained in early passage primary enteroid culture, suggestive of an inherent epithelial phenotype. The Cftr KO proliferative phenotype was apparent through culture passages 1 and 2, but proliferation rates of WT and Cftr KO enteroid crypts converged by passage 4. However, matched WT enteroids at passage 4 assumed a CF-like phenotype with decreased Cftr expression and increased proliferation, ostensibly owing to selection against slower growth by cells (ISCs) expressing higher amounts of Cftr.<sup>42,43</sup> In vivo, the CF intestinal environment may promote epithelial proliferation through disease factors known to increase the risk for GI cancer. One factor is intestinal inflammation; however, studies of small intestinal inflammation in both CF patients and CF mice indicate a relatively mild presentation. Neutrophil and mononuclear cell infiltration of the submucosa are moderate without overt mucosal damage.<sup>5,11</sup> Gene expression studies have indicated immune activation in the small intestine of CF patients.<sup>4,5</sup> In CF mice, changes in innate immunity genes also were noted, but minimized by therapeutic intervention to prevent bowel obstruction by continuously maintaining the mice on a polyethylene glycol

osmotic laxative in the drinking water.<sup>70</sup> CF mice in the present investigation and in the study by Than et al (showing a high incidence of GI tumors)<sup>13</sup> were both maintained on the polyethylene glycol laxative, which may reduce the contribution of inflammation-induced genetic/epigenetic changes. Together with evidence that Cftr is expressed and functional in murine Lgr5+ ISCs, we tentatively conclude that hyperproliferation in the CF intestine is a consequence of losing the growth-suppressive function of Cftr. However, without further investigation, it is difficult to eliminate the possibility that growth stimulation in the Cftr KO enteroids includes epigenetic changes secondary to the CF intestinal environment that are carried into culture.

Wnt/ $\beta$ -catenin signaling is required for proliferation and maintenance of small intestinal stem cells.<sup>28</sup> We found that Wnt/ $\beta$ -catenin signaling, as indicated by active  $\beta$ -catenin and downstream Lef1 protein amounts, is increased in both freshly isolated crypts and early passage enteroids of Cftr KO mice. This finding is consistent with increased numbers of Lgr5+ stem cells in the intestine and enteroids of Cftr KO/Lgr5-EGFP mice. Further studies have shown Cftr protein expression in sorted SOX9<sup>EGFP<sup>Lo</sup></sup> cells, an alkaline pH<sub>i</sub> in Lgr5+-EGFP ISCs in the absence of Cftr activity, and greater proliferation in ISC-enriched enterospheres from Cftr KO mice compared with WT. This evidence supports previous studies identifying CFTR as a downstream target for the terminal effector of Wnt/ $\beta$ -catenin signaling, Tcf4, and suggests that Cftr may play a role in maintaining the balance between intestinal proliferation and differentiation.<sup>46</sup> As a direct target gene, Cftr also may modulate ISC proliferation through actions on the cell cycle. In T and B lymphocyte cell lines, it has been shown that a CFTR-dependent Cl<sup>-</sup> permeability is increased during the G1 phase of the cell cycle, which could be augmented by increasing intracellular cyclic adenosine monophosphate.<sup>71</sup> This coordinates nicely with evidence in other cell types that increased cyclic adenosine monophosphate and reduced intracellular [Cl<sup>-</sup>] during G1 leads to cell-cycle arrest by a p21-dependent mechanism.<sup>72,73</sup> However, potential involvement of Cftr as a growth suppressant in ISC by cell-cycle regulation does not elucidate the pathway of increased Wnt/ $\beta$ -catenin signaling in the crypts of the Cftr KO intestine.

The pathogenesis connecting dysregulated Wnt/ $\beta$ -catenin signaling to the absence of an apical membrane anion channel is unlikely to be direct. Although previous studies have shown CFTR to interact with several proteins thereby affecting various cell processes,<sup>74,75</sup> the undisputed function of CFTR is to provide epithelial Cl<sup>-</sup> and HCO<sub>3</sub><sup>-</sup> permeability. Loss of this permeability in CF disease has been associated with dehydration and reduced pH of the airway and intestinal surfaces, increased mucus viscosity, and deficits of innate immunity.<sup>76–81</sup> Another cellular consequence of CFTR loss is dysregulation of pH<sub>i</sub> in the alkaline range, which recently was shown to be dependent on the combined intracellular retention of Cl<sup>-</sup> and HCO<sub>3</sub><sup>-</sup>.<sup>20</sup> Alkaline pH<sub>i</sub> is conducive to cell proliferation by positive effects on cell-cycle transitions and DNA replication<sup>21,22</sup> and is known to facilitate Wnt signaling by increasing the interaction of Dvl with the inner plasma

membrane to stabilize binding with the Wnt receptor, Fz.<sup>26</sup> Dvl possesses a polycationic motif that targets the protein to the negatively charged inner leaflet, similar to the process used for subcellular localization of a variety of polycationic proteins including K-Ras and proteins associated with endosomes (which show defective recycling in CF cells<sup>82</sup>). Discovered through a genome-wide RNA interference screen of *Drosophila* cells, Dishevelled (Dsh) membrane localization required Na<sup>+</sup>/H<sup>+</sup> exchanger 2 activity to reduce intracellular [H<sup>+</sup>] and improve Fz recruitment of Dsh.<sup>26</sup> Although serial replacement of basic DEP residues indicated that membrane stabilization of Dsh was more important to noncanonical planar cell polarity Wnt signaling than canonical Wnt/ $\beta$ -catenin signaling, it is reasonable that Dvl membrane stabilization by an alkaline pH<sub>i</sub> in CF cells also should facilitate canonical Wnt/ $\beta$ -catenin signaling. Live imaging of enteroids from WT/or Cftr KO/Dvl2 KO/Dvl2-EGFP/Rosa<sup>mT/mG</sup> mice supported this hypothesis by showing greater juxtamembrane association of Dvl in Cftr KO CBC cells. Dvl membrane association was both charge- and pH<sub>i</sub>-dependent and could be predictably manipulated by pharmacologic treatments to reduce intracellular [Cl<sup>-</sup>] in Cftr KO cells or inhibit Cftr in WT cells. Indeed, the acute change in Dvl2-EGFP membrane localization upon alkalization with Cftr<sub>inh</sub>-172 in WT enteroids is more consistent with an epithelial intrinsic effect of Cftr loss on increasing proliferation than genetic/epigenetic effects resulting from life-long absence of Cftr in the Cftr KO model.

The demonstration of greater Dvl association with the plasma membrane in Cftr KO CBCs in situ is consistent with the central hypothesis, but does not directly establish increased Fz-Dvl interaction. Quantitative information regarding the amplification of signal through the cascade of the Wnt/ $\beta$ -catenin pathway and discrete genetic manipulations of an appropriate cell line will be needed to estimate the contribution of Dvl membrane stabilization to increased Wnt/ $\beta$ -catenin signaling. A recent study investigating inflammation in the  $\Delta$ F508 Cftr mouse small intestine concluded, in contradiction to our findings, that loss of Cftr activity suppressed active  $\beta$ -catenin signaling compared with WT.<sup>83</sup> This apparent discrepancy may be methodologic in that our measurements of active  $\beta$ -catenin expression were confined to lysates of freshly isolated crypts to evaluate the proliferative intestinal compartment. In contrast, the study by Liu et al used lysates of whole-thickness small intestine in measurement of total and active  $\beta$ -catenin, which would include the contribution of nonepithelial cell types.<sup>83</sup>

An unexpected outcome in studies of WT CBCs was increased Dvl membrane association at the lateral-Lateral cell membrane. Although the cause of this phenomenon was not investigated, it is tempting to speculate that the lateral-Lateral cell membrane generates a localized pH<sub>i</sub> gradient that increases Dvl localization. Asymmetric cellular pH<sub>i</sub> gradients in intestinal stem cells has largely gone unstudied. However, an asymmetric cellular pH<sub>i</sub> gradient created by Na<sup>+</sup>/H<sup>+</sup> exchanger 1 activity exists at the leading edge of migrating fibroblasts that is necessary for efficient activity of the Rho guanosine triphosphatase Cdc42.<sup>84,85</sup> Cdc42 also plays a critical role in coordinating migration of mouse small intestinal

stem cells.<sup>86</sup> Another potential function for asymmetric Dvl localization also may relate to Dvl's role in mitotic spindle formation,<sup>87</sup> an orderly process that is associated with asymmetric division in normal intestinal stem cells, but not under precancerous conditions (eg, APC<sup>min</sup> mice).<sup>88</sup>

Increased Dvl association with the supranuclear lateral plasma membrane in Cftr KO crypt epithelium may facilitate noncanonical Wnt pathways of planar cell polarity and directional cell movement.<sup>89,90</sup> Increased cell migration from the crypts as a consequence of increased epithelial proliferation has been shown in the Cftr KO mouse in vivo.<sup>14</sup> In intestinal crypts, cell migration must be closely coordinated with proliferation and involves remodeling of the adherens junctions by processes that are not well understood in this context.<sup>91</sup> Dvl is a crucial component of the planar cell polarity pathway as previously shown for polarized cell migration of mouse embryonic fibroblasts.<sup>92</sup> Dvl transduces signals from Wnt-liganded Fz and the co-receptor Ror2, a tyrosine kinase-like orphan receptor, which directs c-Jun N-terminal kinase for activation of c-Jun, resulting in cytoskeletal reorganization and polarized cell migration.<sup>27</sup> Studies in *Xenopus* have shown that polarization of ectodermal cells involves *Xenopus* disheveled (xDsh) accumulation with Fz7 at the apical adherens junctions in response to Wnt11.<sup>93</sup> Dvl also may provide a link between the Fz/Ror2 pathway and Cdc42 for polarized cell migration. The Rho family guanosine triphosphatase Cdc42 is a major determinant of apical-basal polarity in intestinal epithelium.<sup>86</sup> Cdc42 is recruited by guanine exchange factors, a process facilitated by an alkaline pH<sub>i</sub>,<sup>85</sup> and can bind partitioning complex members Par3 and Par6 at the tight junctional complex and apical membrane, respectively.<sup>94</sup> This process leads to activation of an atypical protein kinase C (aPKC, PKC $\zeta$ ), potentially regulated by the DEP domain of Dvl,<sup>27</sup> which facilitates polarized cell migration.<sup>95</sup> Additional studies will be necessary to sort out the cellular processes that coordinate crypt cell proliferation with crypt cell migration.

In conclusion, our data show that the absence of Cftr activity in murine ISCs establishes an alkaline pH<sub>i</sub> that potentially facilitates canonical Wnt/ $\beta$ -catenin signaling by increasing the stability of the Wnt transducer Dvl at the plasma membrane. The rate of ISC proliferation and changes of signaling in the Cftr KO intestine are moderate, but over the course of a lifetime create an insidious process that is predicted to increase the risk of intestinal carcinogenesis. When placed within the context of the Cftr KO intestinal environment, with attendant inflammation and dysbiosis, a significant risk for neoplasia develops that is consistent with the high tumor penetrance (~60%) showed by aged CF mice.<sup>13</sup> However, epithelial proliferation rates and Wnt/ $\beta$ -catenin signaling of the intestine in CF patients has largely gone unstudied. These data from the Cftr KO mouse model should illuminate the need to investigate this potential risk factor in CF. With continued improvements in care and an aging CF population, the incidence of digestive tract cancer likely will increase. There is a need for more attention to clinical screening of CF patients for GI cancer and investigations identifying the underlying processes by which

life-long dysfunction of an epithelial anion channel yields increased gastrointestinal cancer risk.

## References

- Anderson MP, Gregory RJ, Thompson S, Souza DW, Paul S, Mulligan RC, Smith AE, Welsh MJ. Demonstration that CFTR is a chloride channel by alteration of its anion selectivity. *Science* 1991;253:202–205.
- Poulsen JH, Fischer H, Illek B, Machen TE. Bicarbonate conductance and pH regulatory capability of cystic fibrosis transmembrane conductance regulator. *Proc Am Acad Sci U S A* 1994;91:5340–5344.
- Norkina O, Burnett TG, De Lisle RC. Bacterial overgrowth in the cystic fibrosis transmembrane conductance regulator null mouse small intestine. *Infect Immun* 2004;72:6040–6049.
- Smyth RL, Croft NM, O’Hea U, Marshall TG, Ferguson A. Intestinal inflammation in cystic fibrosis. *Arch Dis Child* 2000;82:394–399.
- Raia V, Maiuri L, De Ritis G, De Vizia B, Vacca L, Conte R, Auricchio A, Londei M. Evidence of chronic inflammation in morphologically normal small intestine of cystic fibrosis patients. *Pediatr Res* 2000;47:344–350.
- Welsh MJ, Tsui LC, Boat TF, Beaudet AL. Cystic fibrosis. In: Scriver CR, Beaudet AL, Sly WS, Valle D, Fredrickson DS, eds. *Metabolic and molecular basis of inherited disease*, Vol 7. New York: McGraw Hill, 1995:3799–3863.
- Borowitz D, Durie PR, Clarke LL, Werlin SI, Taylor CJ, Semier J, De Lisle RC, Lewindon P, Lichtman SM, Sinaasappel M, Baker RD, Baker SS, Verkade HJ, Lowe ME, Stallings VA, Janhorbani M, Bulter R, Heubi J. Gastrointestinal outcomes and confounders in cystic fibrosis. *J Pediatr Gastroenterol Nutr* 2005;41:273–285.
- Maisonneuve P, Fitzsimmons SC, Neglia JP, Campbell PW, Lowenfels AB. Cancer risk in non-transplanted and transplanted cystic fibrosis patients: a 10-year study. *J Natl Cancer Inst* 2003;95:381–387.
- Neglia JP, Fitzsimmons SC, Maisonneuve P, Schoni MH, Schoni-Affolter F, Corey M, Lowenfels AB. The risk of cancer among patients with cystic fibrosis. *N Engl J Med* 1995;332:494–499.
- Snouwaert JN, Brigman KK, Latour AM, Malouf NN, Boucher RC, Smithies O, Koller BH. An animal model for cystic fibrosis made by gene targeting. *Science* 1992;257:1083–1088.
- Norkina O, Kaur S, Ziemer D, De Lisle RC. Inflammation of the cystic fibrosis mouse small intestine. *Am J Physiol Gastrointest Liver Physiol* 2004;286:G1032–G1041.
- Clarke LL, Gawenis LR, Bradford EM, Judd LM, Boyle KT, Simpson JE, Shull GE, Tanabe H, Ouellette AJ, Franklin CL, Walker NM. Abnormal Paneth cell granule dissolution and compromised resistance to bacterial colonization in the intestine of CF mice. *Am J Physiol Gastrointest Liver Physiol* 2004;286:G1050–G1058.
- Than BLN, Linnekamp JF, Starr TK, Largaespada DA, Rod A, Zhang Y, Bruner V, Abrahante J, Schumann A, Luczak T, Niemczyk A, O’Sullivan MG, Medema JP, Fijneman RJA, Meijer GA, Ban den Broek E, Hodges CA, Scott PM, Vermeulen L, Cormier RT. CFTR is a tumor suppressor gene in murine and human intestinal cancer. *Oncogene* 2016;35:4179–4187.
- Gallagher AM, Gottlieb RA. Proliferation, not apoptosis, alters epithelial cell migration in small intestine of CFTR null mice. *Am J Physiol Gastrointest Liver Physiol* 2001;281:G681–G687.
- Tomasetti C, Vogelstein B. Variation in cancer risk among tissues can be explained by the number of stem cell divisions. *Science* 2015;347:78–81.
- Tomasetti C, Li L, Vogelstein B. Stem cell divisions, somatic mutations, cancer etiology, and cancer prevention. *Science* 2017;355:1330–1334.
- Strong TV, Boehm K, Collins FS. Localization of cystic fibrosis transmembrane conductance regulator mRNA in the human gastrointestinal tract by in situ hybridization. *J Clin Invest* 1994;93:347–354.
- Ameen NA, Alexis J, Salas P. Cellular localization of the cystic fibrosis transmembrane conductance regulator in mouse intestinal tract. *Histochem Cell Biol* 2000;114:69–75.
- Liu J, Walker NM, Cook MT, Ootani A, Clarke LL. Functional Cfr in crypt epithelium of organotypic enteroid cultures from murine small intestine. *Am J Physiol Cell Physiol* 2012;302:C1492–C1503.
- Walker NM, Liu J, Stein SR, Stefanski CD, Strubberg AM, Clarke LL. Cellular chloride and bicarbonate retention alters intracellular pH regulation in Cfr KO crypt epithelium. *Am J Physiol Gastrointest Liver Physiol* 2016;310:G70–G80.
- Putney LK, Barber DL. Na-H exchange-dependent increase in intracellular pH times  $G_2/M$  entry and transition. *J Biol Chem* 2003;278:44645–44649.
- Schreiber R.  $Ca^{2+}$  signaling, intracellular pH and cell volume in cell proliferation. *J Membr Biol* 2005;205:129–137.
- Casey JR, Grinstein S, Orlowski J. Sensors and regulators of intracellular pH. *Nat Rev Mol Cell Biol* 2010;11:50–61.
- Webb BA, Chimenti M, Jacobson MP, Barber DL. Dysregulated pH: a perfect storm for cancer progression. *Nat Rev Cancer* 2011;11:671–677.
- Young BP, Shin JJH, Orij R, Chao JT, Li SC, Guan SL, Khong A, Jan E, Wenk MR, Prinz WA, Smits GJ, Loewen CJR. Phosphatidic acid is a pH biosensor that links membrane biogenesis to metabolism. *Science* 2010;329:1085–1088.
- Simons M, Gault WJ, Gotthardt D, Rohatgi R, Klein TJ, Shao Y, Lee HJ, Wu AL, Fang Y, Satlin LM, Dow JT, Chen J, Zheng J, Boutros M, Mlodzik M. Electrochemical cues regulate assembly of the Frizzled/Dishevelled complex at the plasma membrane during planar epithelial polarization. *Nat Cell Biol* 2009;11:286–294.
- Gao C, Chen YG. Dishevelled: the hub of Wnt signaling. *Cell Signal* 2010;22:717–727.
- Fevr T, Robine S, Louvard D, Huelsken J. Wnt/beta-catenin is essential for intestinal homeostasis and maintenance of intestinal stem cells. *Mol Cell Biol* 2007;27:7551–7559.

29. De Lisle RC, Mueller R, Boyd M. Impaired mucosal barrier function in the small intestine of the cystic fibrosis mouse. *J Pediatr Gastroenterol Nutr* 2011; 53:371–379.
30. Sato T, Vries RG, Snippert HJ, van de Wetering M, Barker N, Strange DE, van Es JH, Abo A, Kujala P, Peters PJ, Clevers H. Single Lgr5 stem cells build crypt-villus structures in vitro without a mesenchymal niche. *Nature* 2009;459:262–265.
31. Lee Y-N, Gao Y, Wang H-Y. Differential mediation of the Wnt canonical pathway by mammalian Dishevelleds-1, -2, and -3. *Cell Signal* 2008;20:443–452.
32. Etheridge SL, Ray S, Li S, Hamblet NS, Lijam N, Tsang M, Greer J, Kardos N, Wang J, Sussman DJ, Cjem P, Wynshaw-Boris A. Murine Dishevelled 3 functions in redundant pathways with Dishevelled 1 and 2 in normal cardiac outflow tract, cochlea, and neural tube development. *PLoS Genet* 2008;4:e1000259.
33. Clarke LL, Gawenis LR, Franklin CL, Harline MC. Increased survival of CFTR knockout mice using an oral osmotic laxative. *Lab Animal Sci* 1996;46:612–618.
34. Wang J, Hamblet NS, Mark S, Dickinson ME, Binkman BC, Segil N, Fraser SE, Chen P, Wallingford JB, Wynshaw-Boris A. Dishevelled genes mediate a conserved mammalian PCP pathway to regulate convergent extension during neurulation. *Development* 2006;133:1767–1778.
35. Liu J, Lu W, Guha S, Baltazar GC, Coffey EE, Laties AM, Rubenstein RC, Reenstra WW, Mitchell CH. Cystic fibrosis transmembrane conductance regulator (CFTR) contributes to reacidification of alkalized lysosomes in RPE cells. *Am J Physiol Cell Physiol* 2012; 303:C160–C169.
36. Formeister EJ, Sionas AL, Lorange DK, Barkley CL, Lee GH, Magness ST. Distinct SOX9 levels differentially mark stem/progenitor populations and enteroendocrine cells of the small intestine epithelium. *Am J Physiol Gastrointest Liver Physiol* 2009;296:G1108–G1118.
37. Simpson JE, Gawenis LR, Walker NM, Boyle KT, Clarke LL. Chloride conductance of CFTR facilitates basal  $\text{Cl}^-/\text{HCO}_3^-$  exchange in the villous epithelium of intact murine duodenum. *Am J Physiol Gastrointest Liver Physiol* 2005;288:G1241–G1251.
38. Ootani A, Li X, Sangiorgi E, Ho QT, Ueno H, Toda S, Sugihara H, Fujimoto K, Weissman IL, Capecchi MR, Kuo CJ. Sustained in vitro intestinal epithelial culture within a Wnt-dependent stem cell niche. *Nat Med* 2009; 15:701–706.
39. Barker N, Van Es JH, Kuipers J, Kujala P, Van der Born M, Cozijnsen M, Haegebarth A, Korving J, Begthel H, Peters PJ, Clevers H. Identification of stem cells in small intestine and colon by marker gene Lgr5. *Nature* 2007;449:1003–1008.
40. Karrasch T, Spaeth T, Allard B, Jobin C. PI3K-dependent GSK3s(Ser9)-phosphorylation is implicated in the intestinal epithelial cell wound-healing response. *PLoS One* 2011;6:e26340.
41. Diks SH, Hardwick JC, Diab RM, van Santen MM, Versteeg HH, van Deventer SJH, Richel DJ, Peppelenbosch MP. Activation of the canonical  $\beta$ -catenin pathway by histamine. *J Biol Chem* 2003; 278:52491–52496.
42. Clarke LL, Gawenis LR, Hwang TC, Walker NM, Gruis DB, Price EM. A domain mimic increases DF508 CFTR trafficking and restores cAMP-stimulated anion secretion in cystic fibrosis epithelia. *Am J Physiol Cell Physiol* 2004;287:C192–C199.
43. Schiavi SC, Abdelkader N, Reber S, Pennington S, Narayana R, McPherson JM, Smith AE, Hoppe IH, Cheng SH. Biosynthetic and growth abnormalities are associated with high-level expression of CFTR in heterologous cells. *Am J Physiol Cell Physiol* 1996; 270:C341–C351.
44. van Noort M, Meeldijk J, van der Zee R, Destree O, Clevers H. Wnt signaling controls the phosphorylation status of  $\beta$ -catenin. *J Biol Chem* 2002;277:17901–17905.
45. van der Flier LG, Sabates-Bellver J, Oving I, Haegebarth A, De Palo M, Anti M, Van Gijn ME, Suijkerbuijk S, De Wetering MV, Marra G, Clevers H. The intestinal Wnt/TCF signature. *Gastroenterology* 2007; 132:628–632.
46. Paul T, Li S, Khurana S, Leleiko NS, Walsh MJ. The epigenetic signature of CFTR expression is co-ordinated via chromatin acetylation through a complex intronic element. *Biochem J* 2007;408:317–326.
47. Gracz AD, Ramalingam S, Magness ST. Sox9 expression marks a subset of CD24-expressing small intestine epithelial stem cells that form organoids in vitro. *Am J Physiol Gastrointest Liver Physiol* 2010; 298:G590–G600.
48. Hirokawa M, Takeuchi T, Chu S, Akiba Y, Wu V, Guth PH, Engel E, Montrose MH, Kaunitz JD. Cystic fibrosis gene mutation reduces epithelial cell acidification and injury in acid-perfused mouse duodenum. *Gastroenterology* 2004;127:1162–1173.
49. Elgavish A. High intracellular pH in CFPAC: a pancreas cell line from a patient with cystic fibrosis is lowered by retrovirus-mediated CFTR gene transfer. *Biochem Biophys Res Commun* 1991;180:342–348.
50. Stelzner M, Helmrath M, Dunn JCY, Henning SJ, Houchen CW, Kuo C, Lynch J, Li L, Magness ST, Martin MG, Wong MH, Yu J. A nomenclature for intestinal in vitro cultures. *Am J Physiol Gastrointest Liver Physiol* 2012;302:G1359–G1363.
51. VanDussen KL, Marinshaw JM, Miyoshi H, Ciorba MA, Stappenbeck TS. Efficient isolation, expansion and differentiation of human epithelial stem cells from endoscopic biopsies of the gastrointestinal tract. *Gastroenterology* 2013;144:S62–S63.
52. Miyoshi H, Stappenbeck TS. In vitro expansion and genetic modification of gastrointestinal stem cells in spheroid culture. *Nat Protoc* 2013;8:2471–2482.
53. Sato T, Stange DE, Ferrante M, Vries RGJ, van Es JH, van den Brink S, van Houdt WJ, Pronk A, van Gorp J, Siersema PD, Clevers H. Long-term expansion of epithelial organoids from human colon, adenoma, adenocarcinoma, and Barrett's epithelium. *Gastroenterology* 2011;141:1762–1772.
54. Yin X, Farin HF, van Es JH, Clevers H, Langer R, Karp JM. Niche-independent high-purity cultures of

- Lgr5+ intestinal stem cells and their progeny. *Nat Methods* 2014;11:106–112.
55. Dekkers JF, Wiegerinck CL, de Jonge HR, Bronsveld I, Jassens HM, de Winger-de Groot KM, Brandsma AM, de Jong NWM, Bijvelds MJC, Scholte BJ, Nieuwenhuis EES, van den Brink S, Clevers H, van der Ent CK, Middendorp S, Beekman JM. A functional CFTR assay using primary cystic fibrosis intestinal organoids. *Nat Med* 2013;19:939–945.
  56. Grumolato L, Liu G, Mong P, Mudbhary R, Biswas R, Arroyave R, Vijayakumar S, Economides AN, Aaronson SA. Canonical and noncanonical Wnts use a common mechanism to activate completely unrelated coreceptors. *Gene Dev* 2010;24:2517–2530.
  57. Pan WJ, Pang SZ, Huang T, Guo HY, Wu D, Li L. Characterization of function of three domains in dishevelled-1: DEP domain is responsible for membrane translocation of dishevelled-1. *Cell Res* 2004;14:324–330.
  58. Flanagan DJ, Phesse TJ, Barker N, Schwab RH, Amin N, Malaterre J, Strange DE, Nowell CJ, Currie SA, Saw JT, Beuchert E, Ramsay RG, Sansom OJ, Ernst M, Clevers H, Vincan E. Frizzled7 functions as a Wnt receptor in intestinal epithelial Lgr5(+) stem cells. *Stem Cell Rep* 2015;4:759–767.
  59. Wang W, Anderson NA, Travesset A, Vaknin D. Regulation of the electric charge in phosphatidic acid domains. *J Phys Chem B* 2012;116:7213–7220.
  60. Fitzgerald RC, Omary MB, Triadafilopoulos G. Acid modulation of HT29 cell growth and differentiation. *J Cell Sci* 1997;110:663–671.
  61. Liu X, Luo M, Zhang L, Ding W, Yan Z, Engelhardt JF. Bioelectric properties of chloride channels in human, pig, ferret, and mouse airway epithelia. *Am J Respir Cell Mol* 2007;36:313–323.
  62. Gory I, Brown G, Wilson J, Kemp W, Paul E, Roberts SK. Increased risk of colorectal neoplasia in adult patients with cystic fibrosis: a matched case-control study. *Scand J Gastroenterol* 2014;49:1230–1236.
  63. Inoue K, Fry EA, Taneja P. Recent progress in mouse models for tumor suppressor genes and its implications in human cancer. *Clin Med Insights Oncol* 2013;7:103–122.
  64. Aparicio T, Zaanan A, Svrcek M, Laurent-Puig P, Carrere N, Manfredi A, Locher C, Afchain P. Small bowel adenocarcinoma: epidemiology, risk factors, diagnosis and treatment. *Dig Liver Dis* 2014;46:97–104.
  65. Shenoy S. Genetic risks and familial associations of small bowel carcinoma. *World Gastrointest Oncol* 2016;8:509–519.
  66. Garg M, Ooi CY. The enigmatic gut in cystic fibrosis: linking inflammation, dysbiosis, and the increased risk of malignancy. *Curr Gastroenterol Rep* 2017;19:6.
  67. Manor O, Levy R, Pope CE, Hayden HS, Brittnacher MJ, Carr R, Radey MC, Hager KR, Heltshe SL, Ramsey BW, Miller SI, Hoffman LR, Borenstein E. Metagenomic evidence for taxonomic dysbiosis and functional imbalance in the gastrointestinal tracts of children with cystic fibrosis. *Sci Rep* 2016;6:22493.
  68. Lynch SV, Goldfarb KC, Wild YK, Kong W, De Lisle RC, Brodie EL. Cystic fibrosis transmembrane conductance regulator knockout mice exhibit aberrant gastrointestinal microbiota. *Gut Microbes* 2013;4:41–47.
  69. Qazi TM, O'Brien MJ, Farraye FA, Gould RW, Chen CA, Schroy PC 3rd. Epidemiology of goblet cell and microvesicular hyperplastic polyps. *Am J Gastroenterol* 2014;109:1922–1932.
  70. De Lisle RC, Roach E, Jansson K. Effects of laxative and N-acetylcysteine on mucus accumulation, bacterial load, transit, and inflammation in the cystic fibrosis mouse small intestine. *Am J Physiol Gastrointest Liver Physiol* 2007;293:G577–G584.
  71. Bubien JK, Kirk KL, Rado TA, Frizzell RA. Cell cycle dependence of chloride permeability in normal and cystic fibrosis lymphocytes. *Science* 1990;248:1416–1419.
  72. Miyazaki H, Shiozaki A, Niisato N, Ohsawa R, Itoi H, Ueda Y, Otsuji E, Yamagishi H, Iwasaki Y, Nakano T, Nakahari T, Marunaka Y. Chloride ions control the G1/S cell-cycle checkpoint by regulating the expression of p21 through a p53-independent pathway in human gastric cancer cells. *Biochem Biophys Res Commun* 2008;366:506–512.
  73. Zeilig CE, Goldberg ND. Cell-cycle-related changes of 3': 5'-cyclic GMP levels in Novikoff hepatoma cells. *Proc Natl Acad Sci U S A* 1977;74:1052–1056.
  74. Ko SBH, Zeng W, Dorwart MR, Luo X, Kim KH, Millen L, Goto H, Naruse S, Soyombo A, Thomas PJ, Muallem S. Gating of CFTR by the STAS domain of SLC26 transporters. *Nat Cell Biol* 2004;6:343–350.
  75. Rymut SM, Harker A, Corey DA, Burgess JD, Sun H, Clancy JP, Kelley TJ. Reduced microtubule acetylation in cystic fibrosis epithelial cells. *Am J Physiol Lung Cell Mol Physiol* 2013;305:L419–L431.
  76. Coakley RD, Grubb BR, Paradiso AM, Gatzky JT, Johnson LG, Kreda SM, O'Neal WK, Boucher RC. Abnormal surface liquid pH regulation by cultured cystic fibrosis bronchial epithelium. *Proc Natl Acad Sci U S A* 2003;100:16083–16088.
  77. Henderson AG, Ehre C, Button B, Abdullah LH, Cai L-H, Leigh MW, DeMaria GC, Matsui H, Donaldson SH, Davis CW, Sheehan JK, Boucher RC, Kesimer Mehmet. Cystic fibrosis airway secretions exhibit mucin hyperconcentration and increased osmotic pressure. *J Clin Invest* 2014;124:3047–3060.
  78. Li X, Tang XX, Vargas Buonfiglio LG, Comelias AP, Ramachandran S, Karp PH, Taft PJ, Sheets K, Abou Alaiwa MH, Welsh MJ, Meyerholz DK, Stoltz DA, Zabner J. Electrolyte transport properties in distal small airways from cystic fibrosis pigs with implications for host defense. *Am J Physiol Lung Cell Mol Physiol* 2016;310:L670–L679.
  79. Abou Alaiwa MH, Beer AM, Pezzulo AA, Launspach JL, Horan RA, Stoltz DA, Stamer TD, Welsh MJ, Zabner J. Neonates with cystic fibrosis have a reduced nasal liquid pH; a small pilot study. *J Cyst Fibros* 2014;13:373–377.
  80. Pezzulo AA, Tang XX, Hoegger MJ, Abou Alaiwa MH, Ramachandran S, Moninger TO, Karp PH, Wohlford-Lenane CL, Haagsman HP, van Eijk M, Banfi B, Horswill AR, Stoltz DA, McCray PB, Welsh MJ, Zabner J. Reduced airway surface pH impairs bacterial killing in the porcine cystic fibrosis lung. *Nature* 2012;487:109–113.

81. Kaur S, Norkina O, Ziemer D, Samuelson LC, De Lisle RC. Acidic duodenal pH alters gene expression in the cystic fibrosis mouse pancreas. *Am J Physiol Gastrointest Liver Physiol* 2004;287:G480–G490.
82. Bradbury NA, Jilling T, Berta G, Sorscher EJ, Bridges RJ, Kirk KL. Regulation of plasma membrane recycling by CFTR. *Science* 1992;256:530–532.
83. Liu KZ, Zhang JT, Tsang LL, Jiang X, Chan HC. Defective CFTR- $\beta$ -catenin interaction promotes NF- $\kappa$ B nuclear translocation and intestinal inflammation in cystic fibrosis. *Oncotarget* 2016;7:64030–64042.
84. Denker SP, Barber DL. Cell migration requires both ion translocation and cytoskeletal anchoring by the Na-H exchanger NHE1. *J Cell Biol* 2002;159:1087–1096.
85. Frantz C, Karydis A, Nalbant P, Hahn KM, Barber DM. Positive feedback between Cdc42 activity and H<sup>+</sup> efflux by the Na-H exchanger NHE1 for polarity of migrating cells. *J Cell Biol* 2007;179:403–410.
86. Melendez J, Liu M, Sampson L, Akunuru S, Han X, Vallance J, Witte D, Shroyer N, Zheng Y. Cdc42 coordinates proliferation, polarity, migration, and differentiation of small intestinal epithelial cells in mice. *Gastroenterology* 2013;145:808–819.
87. Kikuchi K, Niikura Y, Kitagawa K, Kikuchi A. Dishevelled, a Wnt signalling component, is involved in mitotic progression in cooperation with Plk1. *EMBO J* 2010;29:3470–3483.
88. Quyn AJ, Appleton PL, Carey FA, Steele FR, Barker N, Clevers H, Ridgway RA, Sansom OJ, Nathke IS. Spindle orientation bias in gut epithelial stem cell compartments is lost in precancerous tissue. *Cell Stem Cell* 2010;6:175–181.
89. Park TJ, Gray RS, Sato A, Habas R, Wallingford JB. Subcellular localization and signaling properties of dishevelled in developing vertebrate embryos. *Curr Biol* 2005;15:1039–1044.
90. Novellasmunt L, Antas P, Li VS. Targeting Wnt signaling in colorectal cancer. A review in the theme: cell signaling: proteins, pathways and mechanisms. *Am J Physiol Cell Physiol* 2015;309:C511–C521.
91. Madara J, Trier J. The functional morphology of the mucosa of the small intestine. In: . In: Johnson L, ed. *Physiology of the gastrointestinal tract*. 3rd ed, Vol 2. New York: Raven Press, 1994:1577–1622.
92. Nishita M, Yoo SK, Nomachi A, Kani S, Sougawa N, Ohta Y, Takada S, Kikuchi A, Minami Y. Filopodia formation mediated by receptor tyrosine kinase Ror2 is required for Wnt5a-induced cell migration. *J Cell Biol* 2006;175:555–562.
93. Yamanaka H, Nishida E. Wnt11 stimulation induces polarized accumulation of Dishevelled at apical adherens junctions through Frizzled7. *Genes Cells* 2007;12:961–967.
94. Martin-Belmonte F, Gassama A, Datta A, Yu W, Rescher U, Gerke V, Mostov K. PTEN-mediated apical segregation of phosphoinositides controls epithelial morphogenesis through Cdc42. *Cell* 2007;128:383–397.
95. Minami Y, Oishi I, Endo M, Nishita M. Ror-family receptor tyrosine kinases in noncanonical Wnt signaling: their implication in developmental morphogenesis and human diseases. *Dev Dynam* 2010;239:1–15.

---

Received July 5, 2016. Accepted November 18, 2017.

#### Correspondence

Address correspondence to: Lane L. Clarke, DVM, PhD, 324D Dalton Cardiovascular Research Center, University of Missouri, 134 Research Park Drive, Columbia, Missouri 65211-3300. e-mail: [clarkel@missouri.edu](mailto:clarkel@missouri.edu); fax: (573) 884-4232.

#### Acknowledgments

The authors would like to acknowledge the assistance of the Dalton Cardiovascular Research Center Live Cell Imaging Core and Dr Luis Martinez-Lemus (Director).

#### Author contributions

Ashlee M. Strubberg acquired data, analyzed and interpreted data, drafted the manuscript, and critically revised the manuscript; Jinghua Liu acquired data, analyzed and interpreted data, and critically revised the manuscript; Nancy M. Walker acquired data, analyzed and interpreted data, performed the statistical analysis, and provided technical support; Casey D. Stefanski acquired data, analyzed and interpreted data, and provided technical support; R. John MacLeod critically revised the manuscript; Scott T. Magness acquired, analyzed, and interpreted data; and Lane L. Clarke was responsible for the study concept and design, analyzed and interpreted data, critically revised the manuscript, obtained funding, provided administrative support, and supervised the study.

#### Conflicts of interest

The authors disclose no conflicts.

#### Funding

The research was supported by grants from the National Institute of Diabetes and Digestive and Kidney Disease (5R01DK048816 to L.L.C.) and the Cystic Fibrosis Foundation (CLARKE11G0 and CLARKE15G0 to L.L.C., and LIU13Q0 to J.L.).